## Title

Longitudinal Control of Commercial Heavy Vehicles Equipped with Variable Compression Brake



## Authors

Moklegaard, Lasse
Druzhinina, Maria
Stefanopoulou, Anna G.

## Publication Date

2002-03-01

CALIFORNIA PATH PROGRAM
INSTITUTE OF TRANSPORTATION STUDIES
UNIVERSITY OF CALIFORNIA, BERKELEY

# Longitudinal Control of Commercial Heavy Vehicles Equipped with Variable Compression Brake

**Lasse Moklegaard, Maria Druzhinina,**
**Anna G. Stefanopoulou**
*University of Michigan*

**California PATH Research Report**
**UCB-ITS-PRR-2002-13**

This work was performed as part of the California PATH Program of the University of California, in cooperation with the State of California Business, Transportation, and Housing Agency, Department of Transportation; and the United States Department of Transportation, Federal Highway Administration.



Report for MOU 4200

March 2002

ISSN 1055-1425

# Longitudinal Control of Commercial Heavy Vehicles Equipped with Variable Compression Brake

Lasse Moklegaard
Maria Druzhinina
Anna G. Stefanopoulou

Department of Mechanical Engineering
University of Michigan, Ann Arbor, MI 48109-2121

TO 4200 (extension MOU 372)

PATH Research Report

This work was performed as part of the California PATH Program of the University of California, in cooperation with the State of California Business, Transportation, and Housing Agency, Department of Transportation; and the United States Department of Transportation, Federal Highway Administration.



December 2001

# Acknowledgments

This work is supported in part by the California Partners for Advanced Transit and Highways (PATH) under TO 4200.

# Longitudinal Control of Commercial Heavy Vehicles Equipped with Variable Compression Brake

Lasse Moklegaard Maria Druzhinina and Anna G. Stefanopoulou
December 2001

## Abstract

In this report, we extend our previous work within MOU 372 on modeling and longitudinal speed control design for heavy commercial vehicles equipped with a variable compression braking mechanisms. Previously, we developed a detailed crankangle based simulation model for a six cylinder, 350 hp diesel engine with a continuously varying compression brake, that is capable of describing the intrinsic interactions between individual cylinder intake and exhaust processes, turbocharger dynamics during combustion and braking modes, and the transition between those modes. Moreover, for control design and analysis purposes we derived a low-order approximation of that model.

In this report we present our new results on developing longitudinal control algorithms that coordinate the variable compression brake with conventional service brakes and gear selection. Specifically, we integrate the compression brake actuator with the service brakes and design a PI–controller that emulates the driver's actions on long grades. The controller uses the engine speed measurement to activate the service brakes only when retarding power of the compression brake is insufficient. We also employ robust linear control technique using the concept of structured singular values to design a controller that is robust to parameter variations and model uncertainty in the CHV. Finally, we compare the performance of this robust controller with the performance of an adaptive control scheme that we have derived within MOU 393. The performance of all the controllers is demonstrated through extensive simulations on the $24th$ order nonlinear vehicle model developed in our previous work within MOU 372.

## Keywords

Advanced Vehicle Control Systems
Brakes
Commercial Vehicle Operations
Speed Control
Vehicle Dynamics

# Executive Summary

In this report, we extend our previous work within MOU 372 on modeling and longitudinal speed control design for heavy commercial vehicles equipped with a variable compression braking mechanism. CHVs are an essential part of our nation's economy, and an efficient link between marine, railroad and air transportation nodes. Increased highway speed and transportation demands, coupled with limitations in traditional service brake actuators (friction pads on the wheels) create a challenging control problem that requires additional retarding actuators and coordination with service brakes. Although, service brakes can theoretically provide a retarding power ten times higher than the accelerating power of the vehicle, they cannot be used continuously because of the generated heat and associated wear of the friction contacts. The presence of delays associated with the pneumatic or the hydraulic actuation subsystem impose additional constraints on the longitudinal control of CHVs. Faced with these difficulties, fleet and engine manufacturers are introducing additional retarding mechanisms that can provide consistent magnitude and unlimited duration of braking force.

Good and consistent braking for CHVs can be achieved by using an engine compression brake in addition to the conventional friction brakes. The compression brake is a retarding mechanism that enhances braking capability by altering the conventional gas exchange process in the cylinders of the engine and effectively converting the turbocharged diesel engine, that powers the CHV, into a compressor that absorbs kinetic energy from the crankshaft. During compression braking mode the engine dissipates the vehicle kinetic energy through the work done by the pistons to compress the air during the compression stroke. The compressed air is consequently released into the exhaust manifold through a secondary opening of the exhaust valve at the end of the compression stroke. Compression brake increases the overall decelerating capability of the vehicle and, therefore, allows to accommodate higher operational speeds. As a matter of fact, this retarder can potentially be used as a sole decelerating actuator during low deceleration requests. During high deceleration requests it needs to be coordinated with the friction brakes or gear selection to provide sufficient braking power. As a result, the application and intensity of the friction brakes can be reduced and the problems associated with wear and overheating of friction brake actuator can be mitigated. The compression brake is the type of retarding mechanism that we focus on in our work.

Our previous work within MOU 372 contributed to modeling of CHVs [20]-[22]. In particular, we developed a detailed crank angle based simulation model of a diesel engine equipped with a continuously variable compression brake. The variability of the compression braking torque was achieved through controlling a secondary opening of the exhaust valve of the vehicle's turbocharged diesel engine using a variable valve timing actuator. By employing signal processing

to the output of our simulator, we developed a linear reduced order model that is suitable for control design and analysis. That work bridges the gap between the detailed crankangle-based model developed in the engine design community, and the low order representation of engine torque response used in the vehicle dynamics community.

In this report we present our new results on employing classical and modern control techniques to develop longitudinal speed control algorithms that coordinate the variable compression brake with conventional service brakes and gear selection. Since the compression brake can be used continuously without danger of damage and overheating, it is, thus, a natural actuator to be used for speed control.

To guarantee safe and reliable operation of automated vehicles, modern speed control systems need to provide good speed tracking performance and robustness for a multitude of operating conditions such as vehicle mass, road grade, gear combinations, aerodynamic drag, etc. A sensitivity analysis and an evaluation of the model variations and uncertainties across operating regimes, that we carried out in this report, clearly indicate that there is a significant sensitivity to changes in the vehicle payload, gear ratios and road grades. The issue of vehicle load changes is of particular concern in HDV, since the HDV's mass can vary as much as 400 percent (from a configuration of being just a tractor to having one or more trailers) resulting in drastically different closed loop performance. Our initial linear simulations, that we perform using standard Proportional plus Integral (PI) controllers, indicate that these controllers have limited capability to handle large parameter variations and uncertainties of CHVs.

To deal effectively with the large parameter variations and model uncertainty in the CHV we investigate the application of modern robust control methodologies using the concept of structured singular values. In particular, we design a $12th$ order $H_\infty$ controller and a $20th$ order $\mu$–controller using DK iterations that provide robust speed tracking performance and disturbance rejection for a wide variety of operating conditions. We also summarize our work we have done previously within MOU 393 on a model reference nonlinear adaptive controller design to deal with the large variations in vehicle mass and road grade ( see [7], [10]). The performance of the $H_\infty$ and $\mu$-optimal controllers is compared with the performance of the nonlinear adaptive control scheme through extensive simulations on the $24th$ order nonlinear vehicle model developed in our previous work within MOU 372.

In the last part of the report we use a continuously variable compression brake combined with the service brakes during high deceleration requests within longitudinal speed control framework, and investigate the benefits of this coordinated braking controller. Specifically, we design a high priority PI-controller for the compression brake, combined with a P-controller for the service brakes. The priority of the controllers is scheduled based on the saturation of the compression

brake. To quantify the benefits of the developed semi-autonomous, coordinated braking system compared to manually using the service brakes alone, we establish two measures: one that is based on settling time and addresses safety, and one that is related to the use of service brakes and addresses maintenance cost. We show that for one specific critical braking maneuver the coordination of the brakes reduces the use of the service brakes by a factor of 45, and that it reduces the settling time by a factor of 2.

# Contents

**Contents** **vii**

**1 Introduction** **1**

**2 Background on auxiliary retarders** **4**
2.1 Driveline Retarder . . . . . 4
2.2 Exhaust Brake . . . . . 5
2.3 Compression Brake . . . . . 5

**3 Vehicle Model and Sensitivity Analysis** **10**
3.1 Reduced Order Engine Model . . . . . 11
3.2 Longitudinal Vehicle Dynamics . . . . . 13
3.3 Sensitivity Analysis . . . . . 16
3.4 Uncertainty Analysis . . . . . 21
3.4.1 Modeling of Uncertainties . . . . . 22

**4 Control Design** **26**
4.1 Classical Linear Control Design . . . . . 26
4.2 Modern Linear Robust Control Design . . . . . 29
4.2.1 Robustness Analysis . . . . . 31
4.2.2 Robust PI–Controller . . . . . 33
4.2.3 $H_\infty$– Controller . . . . . 35
4.2.4 D–K Iteration Approach . . . . . 36
4.3 Comparative Linear Simulations . . . . . 38
4.4 Nonlinear Control Design . . . . . 40
4.5 Simulations on Full Order Model . . . . . 43
4.5.1 Simulation Implementation . . . . . 45

4.5.2 Speed Tracking: . . . . . 45
4.5.3 Disturbance Rejection . . . . . 47
4.6 Coordination with Gear Selection . . . . . 51
4.7 Conclusion on Control Design . . . . . 54

**5 Coordinated Braking Controller** **55**
5.1 Control Design . . . . . 55
5.2 Simulations on Full Order Model . . . . . 57
5.2.1 Driving Scenario 1: . . . . . 57
5.2.2 Driving Scenario 2: . . . . . 58
5.2.3 Driving Scenario 3: . . . . . 59
5.2.4 Driving Scenario 4: . . . . . 60
5.3 Improvements using Coordination of Brakes . . . . . 61

**6 Conclusions and Future Work** **63**

**Bibliography** **65**

**A Nomenclature** **68**

**B Braking Mode: Parameterization of Dynamics** **71**

# List of Figures


2.1 *Schematic drawing and traces of piston motion and valve lift profiles.* . . . 6
2.2 *Cylinder pressure versus cylinder volume during combustion (dashed), and braking mode (solid).* . . . 8
2.3 *Variable compression braking scheme.* . . . 9
2.4 ***Left:*** *Conventional valve lift system for fixed valve timing.* ***Right:*** *Valve lift system that enables variable valve timing.* . . . 9

3.1 *Steady state map of compression braking torque.* . . . 11
3.2 *Block diagram for reduced order engine model.* . . . 13
3.3 *Block diagram of the vehicle model.* . . . 14
3.4 *Block diagram for linearized vehicle model for braking only.* . . . 16
3.5 *Pole-zero map of the linearized compression brake model.* . . . 17
3.6 *Engine speed time response to step change in brake valve timing.* . . . 18
3.7 *Total gear ratio $r_g$ versus gear number selection.* . . . 19
3.8 *Engine speed response to step change in grade.* . . . 20
3.9 **Perturbation Weight $\mathbf{W}_1$ :** $Relative errors for 45 combinations of M, \omega,$ **and $v_{cb}$ with nominal model.** . . . 24
3.10 **Perturbation Weight $\mathbf{W}_2$ :** $Relative errors for 45 combinations of M, \omega,$ **and $v_{cb}$ with nominal model.** . . . 24

4.1 *Block diagram for compression braking only feedback control system.* . . . 27
4.2 *The closed-loop vehicle performance for step changes in engine speed and road grade using the controller $G_{PI1}$.* . . . 28
4.3 *The closed-loop vehicle performance for step changes in engine speed and road grade using two different PI–controllers.* . . . 29
4.4 *Frequency response for the performance weights.* . . . 32

4.5 *Block diagram of the vehicle system where all the uncertainties are modeled as multiplicative perturbations.* . . . . . 32
4.6 ***Left:*** *General configuration for robust control synthesis.* ***Right:*** *General configuration for robust analysis.* . . . . . 33
4.7 *$\mu$-analysis for $PI_{nom}$ and $PI_{rob}$.* . . . . . 34
4.8 *Reference and disturbance responses for the nominal and the robust PI-controllers, simulated using the linearized vehicle model.* . . . . . 35
4.9 *Reference and disturbance responses for the $H_\infty$–controller.* . . . . . 36
4.10 *$\mu$-analysis for all four controllers.* . . . . . 37
4.11 *Reference and disturbance time responses for the $\mu$–controller.* . . . . . 38
4.12 ***Nominal Vehicle Configuration:*** *Reference and disturbance time responses for all four controllers.* . . . . . 39
4.13 ***Worst Vehicle Configuration:*** *Reference and disturbance time responses for all four controllers.* . . . . . 40
4.14 *Bode plots for all four controllers.* . . . . . 41
4.15 *MRAC's speed tracking performance.* . . . . . 44
4.16 *Block diagram for full nonlinear vehicle model.* . . . . . 45
4.17 ***Nominal Vehicle Configuration:*** *Comparison of the speed reference tracking performances for all the controllers implemented on the full order nonlinear vehicle model.* . . . . . 46
4.18 ***Nominal Vehicle Configuration:*** *Speed reference tracking for all the controllers, here shown in details on the time scale.* . . . . . 48
4.19 ***Nominal Vehicle Configuration:*** *Disturbance rejection capabilities for all the controllers.* . . . . . 49
4.20 ***Worst Vehicle Configuration:*** *Disturbance rejection capabilities for all the controllers.* . . . . . 50
4.21 *For given vehicle mass and engine speed, there is a maximum road grade for what the compression brake can compensate, for each selected gear number.* . . . . . 52
4.22 *Simulation show that the encountered grade is too large for the compression brake to handle for current gear selection, hence, a lower gear number is automatically selected to avoid saturation.* . . . . . 53

5.1 *Block diagram for coordinated braking controller (CBC) scheme.* . . . 56
5.2 *Switching from combustion to braking mode.* . . . . . 57

5.3 ***Driving Scenario 1:*** *Step change in desired engine speed from 157 to 149 rad/sec when operating in braking mode. Results from using the full order nonlinear vehicle model is show as solid lines, while results from using a reduced order model is shown as dotted lines.* . . . . . 58
5.4 ***Driving Scenario 2:*** *Large step in grade while operating braking mode results in saturation of $u_{cb}$ which activates the service brakes.* . . 59
5.5 ***Driving Scenario 3:*** *Transition from combustion to braking mode due to a small step change in grade. Service Brakes are not engaged.* . 60
5.6 ***Driving Scenario 4:*** *Transition from combustion to braking mode due to a large step change in grade. The control output for the compression brake saturates and due to that, the service brakes are activated.* 61
5.7 *Phase plots for driving scenario 1 and 4.* . . . . . 62

B.1 *Regression of compression braking torque.* . . . . . 72
B.2 *Regression of the poles and zeros for the compression brake mode.* . . . 73

# List of Tables

3.1 Range of vehicle parameters. . . . . 21
3.2 Vehicle configuration parameters. . . . . 22

4.1 Standard PI-controller parameters. . . . . 29
4.2 Summary of the $D$–$K$ iteration approach. . . . . 37

B.1 **Braking Mode:** Statistics for regression of poles and zeros. . . . 74

# Chapter 1

# Introduction

Commercial heavy vehicles (CHVs) are an essential part of our nation's economy, and an efficient link between marine, railroad, and air transportation nodes. In 1996, the intercity trucking industry accounted for $176.8 billion in revenues and over 2.9 million jobs [17].

In Automated Highway Systems (AHS), the major goals are to increase highway capacity and to enhance driving safety by automatic longitudinal control of vehicles [4], [25]. Over the last ten years, there has been a significant improvement of the reliability and efficiency of the CHV powertrain. This transformation is primarily achieved by using lightweight material, by reducing aerodynamic drag and frictional losses, and by employing efficient diesel engines. Managers of truck fleets regularly choose diesel engines for their powertrains because they operate at very lean mixtures of fuel and air, and has zero pumping losses. This contributes to the increased fuel economy associated with diesel engines, but on the other hand, it does not provide means for decelerating the moving engine parts. An increase in operational vehicle speed combined with decrease of the natural retarding capabilities in modern powertrains creates challenging braking requirements.

Although conventional service brakes can theoretically provide ten times higher retarding power than acceleration power of the vehicle, they cannot be used continuously due to potential over heating and brake fading of the friction pads in the service brakes [12]. Wear and overheating not only reduce the steady-state authority of the friction brakes but also are a cause of uncertainty in brake operation. In addition, the presence of delays associated with the pneumatic

or hydraulic braking systems impose additional constraint on the longitudinal control of CHVs [27]. Thus, high retarding power with consistent magnitude and unlimited duration is required to be able to maintain operational speed for CHVs that are comparable to passenger vehicles, without compromising safety. Fleet and engine manufactures develop several additional retarding mechanisms to face these requirements. One of the most promising devices is the compression released engine brake, which can be used to increase retarding power to accommodate higher operating speed, and to decrease service brake wear. Since the compression brake can be used continuously without danger of damage and overheating, it is, thus, a natural actuator to be used for speed control. This is the type of retarding mechanism that we focus on in our work.

In our previous work within MOU 372, we developed a detailed crank angle based simulation model of a diesel engine equipped with a continuously variable compression brake [20]-[22]. The variability of the compression braking torque was achieved through controlling a secondary opening of the exhaust valve of the vehicle's turbocharged diesel engine using a variable valve timing actuator. By employing signal processing to the output of our simulator, we developed a linear reduced order model that is suitable for control design and analysis. That work bridges the gap between the detailed crankangle-based model developed in the engine design community, and the low order representation of engine torque response used in the vehicle dynamics community.

In this report we focus on the development of longitudinal control algorithms to regulate the vehicle speed to the desired vehicle speed during descends on long road grades. We employ both classical and modern control techniques for the vehicle model developed in our previous work. Specifically, an initial design of classical linear Proportional plus Integral (PI) controllers is carried out under the assumption that the vehicle system may be approximated with a gain and a first order lag. Initial linear simulations along with the sensitivity analysis indicate that better performance can be achieved using robust and nonlinear controllers. To account for the parameter variations and model uncertainty in the CHV and provide robust speed tracking performance and disturbance rejection for a wide variety of operating conditions we employ robust linear control technique using the concept of structured singular values and nonlinear adaptive control technique. In particular, we design a $12th$ order $H_\infty$-controller and a $20th$ order $\mu$–controller using DK iterations, and also summarize our work we have done

previously within MOU 393 on a model reference adaptive controller design (see [7], [10]). Through extensive simulations, using the $24th$ order nonlinear vehicle model, we demonstrate the performance of the controllers.

In this report we also investigate the benefits of using a continuously variable compression brake combined with the service brakes during high deceleration requests within longitudinal speed control framework. Specifically, we design a high priority PI-controller for the compression brake, combined with a P-controller for the service brakes. The priority of the controllers is scheduled based on the saturation of the compression brake. To quantify the benefits of the developed semi-autonomous, coordinated braking system compared to manually using the service brakes alone, we establish two measures: one that is based on settling time and addresses safety, and one that is related to the use of service brakes and addresses maintenance cost. We show that for one specific critical braking maneuver the coordination of the brakes reduces the use of the service brakes by a factor of 45, and that it reduces the settling time by a factor of 2.

The report is organized as follows. The operating principles of the compression brake as well as two other potential vehicle retarders are described in Chapter 2. In Section 3.1, we review a detailed crankangle-based simulation model of a diesel engine equipped with a compression released engine brake from our previous work [22] and the reduced order approximation of this model for use in control design. We next describe a model for longitudinal vehicle dynamics followed by linearized vehicle model in Section 3.2. A sensitivity analysis in Section 3.3 addresses the necessary development of robust and adaptive control algorithms. In Chapter 4, we develop nominal and robust linear PI–controllers, and $H_\infty$ and $\mu$–optimal controllers, respectively. The uncertainty models needed for the robust design methodology are specified in Section 3.4. These linear controllers are compared with a model reference adaptive controller described in Section 4.4, and the closed-loop performance for all the controllers is demonstrated through simulations using the diesel engine simulator in Section 4.5. A series of driving scenarios demonstrating the improvements obtained by coordinating compression brake and service brakes is presented in Chapter 5. Finally, concluding remarks and directions of future work are made in Chapter 6.

# Chapter 2

# Background on auxiliary retarders

A critical safety issue for CHVs is the vehicle retarding capability. The turbocharged, compression ignition internal combustion (diesel) engine is the preferred powerplant for CHVs. Unlike gasoline engines, diesel engines operate unthrottled, hence, the pistons do not have to work against intake manifold vacuum during the intake stroke. This, combined with very lean mixtures of fuel and air, contributes to the increased fuel economy and to the decreased natural retarding power. The need for higher brake power is addressed by truck manufacturers and fleet managers by the development of various retarding mechanisms in addition to the service brakes (drum or disc brakes on the vehicle wheel). The main categories of these retarders are engine brakes and shaft brakes. In the first category, compression brakes enhance braking efficiency by modifying the conventional gas exchange process. In the second category, shaft retarders are devices attached to the transmission, driveline, or axle that use high turbulence or electro-magnetic forces to dissipate the rotational energy of the moving parts.

Although we will concentrate on the compression brake mechanism in this report, we briefly discuss two other commonly used retarding actuators.

## 2.1 Driveline Retarder

**Hydraulic** driveline retarders are based on the principal of hydraulic coupling and resistance between a rotor attached to the crankshaft or driveline of the

vehicle, and the fins of a stator. Caterpillar and Voith developed manual and automated mechanisms that allow modulated or full braking power, respectively. These mechanisms enable smooth and somewhat controlled braking effort at non-zero rotational speed. Allison driveline retarders apply braking power directly to the driveline and are, therefore, used for stop-and-go driving conditions typical for buses in intercity operation.

**Electric** driveline retarders by Jacobs and Rockwell International, on the other hand, are typically based on dissipating kinetic energy from the driveline by means of setting up a magnetic field. These mechanisms are currently the only ones that allow integration with ABS and ATS.

## 2.2 Exhaust Brake

Exhaust braking is based on an add-on device that restricts the flow out of the exhaust manifold. The result is an increase in the exhaust pressure, which in turn decreases the output power of the engine. The exhaust brake is easy to install, but does not provide high retarding capabilities. Jacobs and Pacific Diesel Brake manufacture this device [2].

## 2.3 Compression Brake

A very promising retarding mechanism is the engine compression brake. This retarder enhances braking capability by altering the conventional gas exchange process in the cylinders of the engine and effectively converting the turbocharged diesel engine, that powers the CHV, into a compressor that absorbs kinetic energy from the crankshaft. During compression braking, fuel injection and combustion are inhibited. Through the work done by the pistons, using the crankshaft kinetic energy, the air in the cylinder is compressed in the compression stroke. At the end of the compression stroke, close to the time when fuel injection usually takes place, the exhaust valve opens dissipating the energy stored in the compressed air into the exhaust manifold.

We call the secondary opening of the exhaust valve the brake valve opening, and refer to the timing of this opening as the brake valve timing (BVT), $v_{cb}$. Due to geometric constraints, the exhaust valve lift profile is considerably different

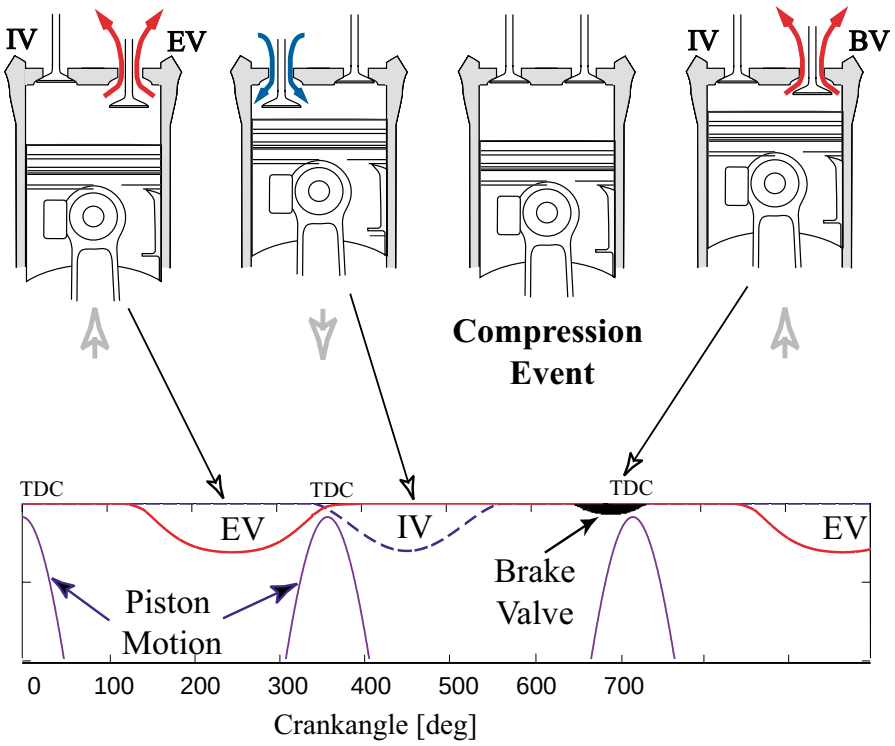


Figure 2.1: *Schematic drawing and traces of piston motion and valve lift profiles.*

for the exhaust and brake events, as shown in Figure 2.1. For simplicity, we call the braking-event profile of the exhaust valve the "brake valve". The activation of the brake valve is typically achieved through a master-slave hydraulic system. The exact profile and timing for the brake valve are designed to maximize the braking power; i.e., to generate the highest peak cylinder pressure. The brake valve profile needs to satisfy constraint on component loading due to high in-cylinder pressure, and geometric clearance between the brake valve trajectory and the piston motion. It is this type of actuator that we focus on in this project.

Figure 2.2 illustrates the valve timing events plotted in a cylinder pressure versus cylinder volume **PV**–diagram. It shows the engine operation during conventional 4-stroke cycle operation (dotted line) and the 4-stroke cycle operation during compression braking (solid line). It is generated using outputs from the model developed in [22], for steady-state engine conditions. Note here that steady-state conditions are defined in a cycle-averaged sense. The engine is considered at steady-state even though its crank angle based behavior is periodic, with one firing or braking cycle as the period. In the **PV**–diagram, the piston

work is positive during combustion and negative during braking, since work is given by

$$W = \oint p_{cyl} dV_{cyl}.$$

Thus, the compression brake is a retarding mechanism that is achieved by inhibiting fuel injection and the combustion event, and, thereby, transforming the engine into a compressor. In that mode, the engine acts like an energy sink [5], because the crankshaft kinetic energy is used to compress the air during the compression stroke. Close to top-dead-center (TDC) the brake valve opens (BVT) and the compressed air is released to the exhaust manifold. Note here that in the absence of BVT all the potential energy stored in the compressed gas will return to the wheels by the downward piston motion. During the brake event, the kinetic energy absorbed during the compression stroke is dissipated as heat in the exhaust manifold. The existing engine cooling system typically manages the dissipation of the exhaust manifold heat and no additional cooling subsystems are introduced to the engine. It is important to note that the engine temperature during braking is not much lower than the one during combustion. As a matter of fact, the overheating of the injectors during braking at long descends is of concern to many engineers. The high temperature in the cylinders can potentially damage the injectors that do not benefit from the cooling effect of the fuel injection during the braking periods.

The concept of compression braking is introduced by Cummins in 1966 [5], and typically depends on an add–on device consisting of a cast iron housing with hydraulic circuitry added on top of the regular engine valve actuator system, that opens the exhaust valve at fixed degrees with respect to the piston motion.

Considerable effort is dedicated to optimize the fixed valve timing to achieve maximum retarding power for all engine speed, load, and environmental conditions. The fixed brake valve timing mechanism is an on-off device and produces a fixed brake torque for a given engine speed. However, for applications in Intelligent Transportation Systems (ITS) full control over the brake valve timing is desirable. A continuously varying brake valve timing allows smooth changes in the compression brake torque response while maintaining constant engine speed. This variability can be used in various CHV applications such as speed regulation, brake-by-wire systems, cruise control, and finally, vehicle-following maneuvers. Moreover, full integration of the compression brake with the service

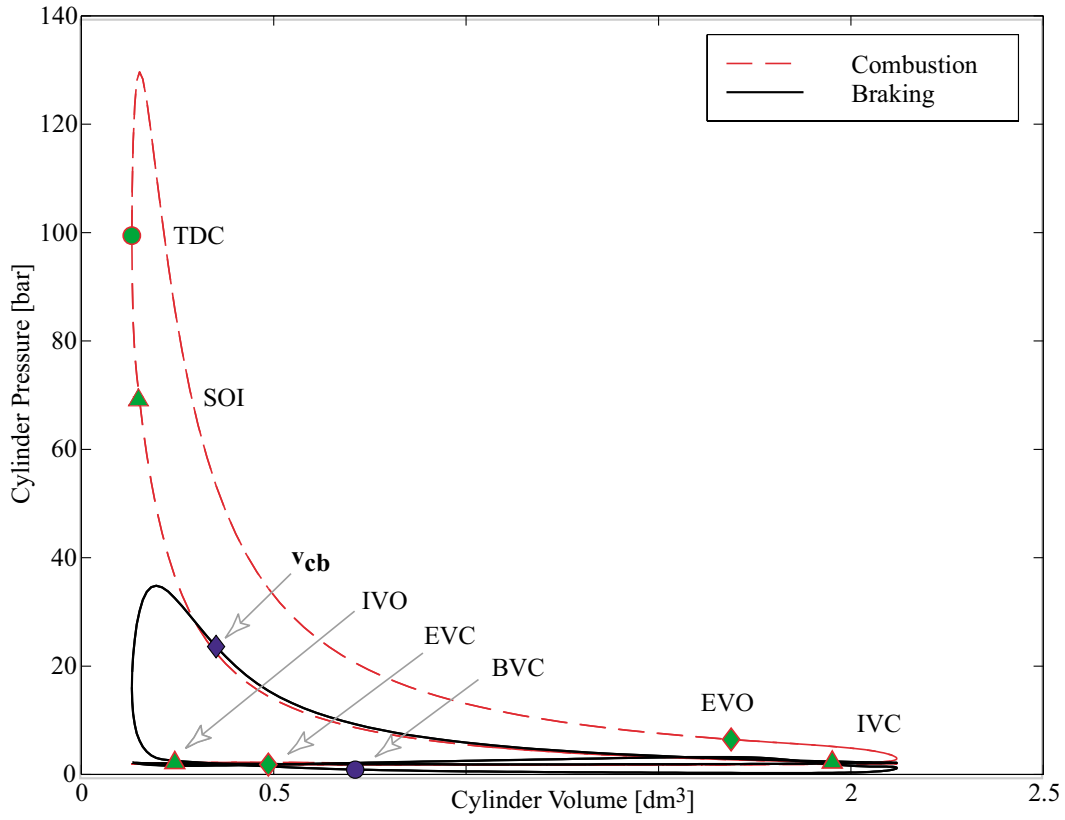


Figure 2.2: *Cylinder pressure versus cylinder volume during combustion (dashed), and braking mode (solid).*

brakes (drum or disc brakes on the vehicle wheel rim) can be achieved. Due to the potential benefits, many engine manufacturers are striving for variable compression braking effort. Work is summarized by Jacobs variable brake valve timing [14], Cummins' discrete cylinder brake valve actuator [15], and Volvo's variable compression braking with exhaust throttle actuator [3].

We define the brake valve timing $v_{cb}$ as the number of crank angle degrees from when the piston is at top-dead-center at the beginning of the intake stroke to the opening of the brake valve at the end of the compression stroke. The following figure, Figure 2.3, shows compression braking power for two different brake valve timings.

Control of the brake valve timing allows us to continuously vary the retarding power of the compression brake mechanism. The left plot in Figure 2.4 shows

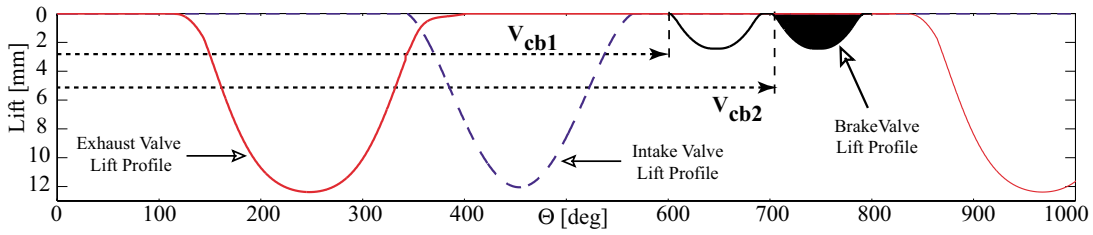


Figure 2.3: *Variable compression braking scheme.*

the fixed activation of the brake valve events based on the mechanical link between the crankshaft and the camshaft. Here, the valve timing is completely determined by the engine speed. The right plot in Figure 2.4, on the other hand, shows a system where the valve is activated by an electro-mechanical or an electro-hydraulic variable valve actuator (VVA). The mechanical connections between the valve profile and the crankshaft are eliminated, allowing a wide continuously variable valve timing.

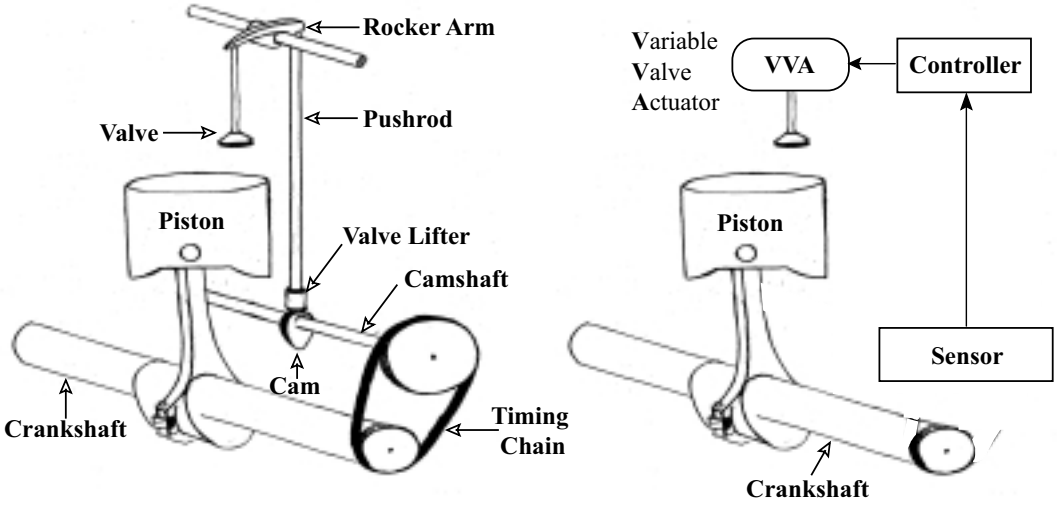


Figure 2.4: ***Left:*** *Conventional valve lift system for fixed valve timing.* ***Right:*** *Valve lift system that enables variable valve timing.*

# Chapter 3

# Vehicle Model and Sensitivity Analysis

In our previous work within MOU 372 we developed a detailed crankangle based simulation model for a six cylinder, 350 Hp diesel engine equipped with a continuously varying compression brake [20]-[22]. The model was based on energy conservation principles in addition to static engine maps provided by the manufacturers, and it was capable of describing the intrinsic interactions between individual cylinder intake and exhaust processes, and turbocharger dynamics during combustion and braking modes and the transition between those modes. Based on averaging and identification of the instantaneous torque response for changes in brake valve timing and fuel flow, we then developed a reduced order, nonlinear dynamic model of the engine as described in Section 3.1.

This reduced model is used in a vehicle model that allows us to perform a sensitivity analysis to determine how mass and gear ratio affect the transient engine speed during step changes in brake valve timing and grade. The analysis indicates a need for robust and nonlinear control design to achieve good vehicle performance for a large range of operating conditions. To prepare for the control design that follows in the next chapter, we specify the uncertainty models needed for the robust design methodology.

## 3.1 Reduced Order Engine Model

We approximate the compression brake torque on the crankshaft, $T_{cb}$ by the following polynomial parameterization (see Figure 3.1):

$$TQ(t) = \alpha_0 + \alpha_1\tilde{\omega}(t) + \alpha_2 W_b(t) + \alpha_3 W_b(t)\tilde{\omega}(t) + \alpha_4\tilde{\omega}(t)^2 + \alpha_5 W_b(t)\tilde{\omega}(t)^2. \tag{3.1}$$

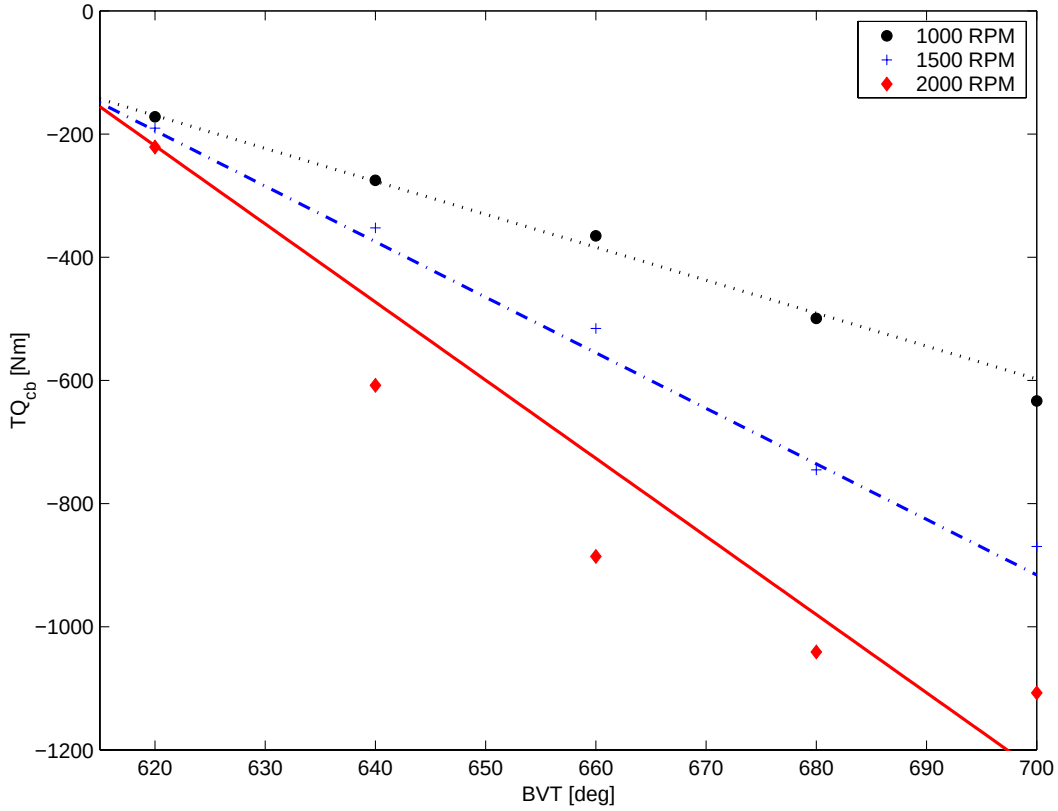


Figure 3.1: *Steady state map of compression braking torque.*

The engine speed dynamics $\tilde{\omega}(t)$ for the engine operating in braking mode is characterized by the following dynamics:

$$\begin{aligned} \tilde{\omega}(t) &= \Delta\tilde{\omega}(t) + \omega_0 \\ \tau_\omega \frac{d}{dt}(\Delta\tilde{\omega}(t)) &= -\Delta\tilde{\omega}(t) + \Delta\omega(t) + c_\omega \frac{d}{dt}(\Delta\omega(t)), \end{aligned} \tag{3.2}$$

where $\omega_0$ is the nominal engine speed, and $\Delta\omega$ is the deviation of the engine speed; i.e. $\Delta\omega(t) = \omega(t) - \omega_0$. The time constant $\tau_\omega$ and the zero $c_\omega$ are given

by the following parameterizations:

$$\tau_\omega = \mathcal{P}_{B1}(\omega_0, W_{b0}) \tag{3.3}$$
$$c_\omega = \mathcal{P}_{B2}(\omega_0, W_{b0}). \tag{3.4}$$

The engine signal $W_b(t)$ is described by the following equations:

$$\begin{aligned} W_b(t) &= \Delta W_b(t) + W_{b0}, \\ \tau \frac{d}{dt}(\Delta W_b(t)) &= -\Delta W_b(t) + \Delta v_{cb}(t) + c\frac{d}{dt}(\Delta v_{cb}(t)) \end{aligned} \tag{3.5}$$

where $W_{b0}$ refers to a nominal engine signal that corresponds to a nominal brake valve timing for the engine. The time constant $\tau$ and the zero $c$ are given by the following parameterizations:

$$\tau = \mathcal{P}_{B3}(\omega_0, W_{b0}) \tag{3.6}$$
$$c = \mathcal{P}_{B4}(\omega_0, W_{b0}). \tag{3.7}$$

The input $\Delta v_{cb}$, in (3.5), denotes the commanded brake valve timing from the variable valve actuator (VVA). The equation that describes the dynamics of $\Delta v_{cb}$, is given by:

$$\tau_a \frac{d}{dt}(\Delta v_{cb}(t)) = -\Delta v_{cb}(t) + \Delta u_{cb}(t), \tag{3.8}$$

where $\Delta u_{cb}(t)$ is the deviation output of the vehicle controller $u_{cb}(t)$, and $\tau_a$ is the time constant of the valve actuator.

Currently, the conventional devices have a fixed time constant $\tau_a$ of approximately 0.6 seconds. This is the time necessary to pump–up the system's hydraulic pressure sufficiently to open the brake valve against the high cylinder pressure. This means that the actuator dynamics will dominate the engine dynamics. However, the new generation variable compression braking mechanisms are expected to be in the order of $10^{-2}$ seconds, hence, the engine dynamics just identified will be dominating.

Under the assumption that $\tau_a \ll \tau$ and $\tau_a \ll \tau_\omega$, the deviation output from the vehicle controller $\Delta u(t)$ is the same as the commanded brake valve timing $\Delta v_{cb}$; i.e.

$$\Delta v_{cb}(t) = \Delta u_{cb}(t) \tag{3.9}$$

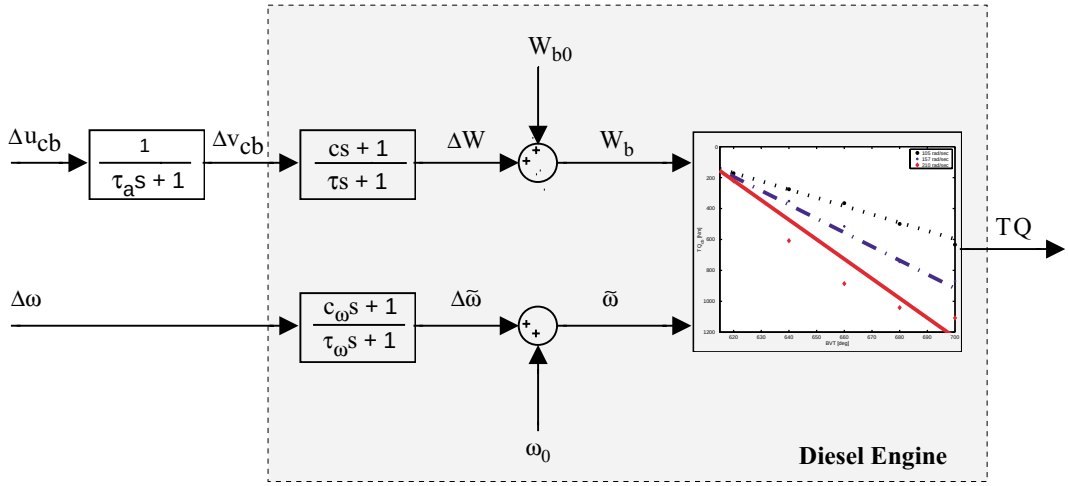


Figure 3.2: *Block diagram for reduced order engine model.*

## 3.2 Longitudinal Vehicle Dynamics

Newton's second law applied to a single inertial mass lumped parameter model (neglecting slip) is used to describe the longitudinal dynamics for a class-8 commercial heavy vehicle:

$$J_t\dot{\omega} = TQ + r_g(F_\beta - F_{sb} - F_a). \tag{3.10}$$

The engine rotational speed $\omega$ (rad/sec) is related to the vehicle speed $v$ (m/sec) the following way:

$$v = \omega\, r_g, \tag{3.11}$$

where the total gear ratio $r_g = \frac{r_w}{g_t g_{fd}}$ depends on the wheel diameter $r_w$, and the transmission and final drive gear ratio $g_t$, and $g_{fd}$, respectively. The total vehicle inertia $J_t$ reflected on the engine shaft depends on total vehicle mass $M$ (kg), the engine inertia $I_e$ and the total gear ratio $r_g$:

$$J_t = Mr_g^2 + I_e. \tag{3.12}$$

In $F_\beta$, we combine the effect of gravitational force due to road grade $\beta$ (where we assume that $\beta < 0$ for descending grades), with rolling resistance $f_r$ forces:

$$F_\beta = -r_g Mg(\cos\beta - f_r \sin\beta). \tag{3.13}$$

The aerodynamic force $F_a$ that depends on the drag coefficient $c_d$, the frontal area $A$, and the air density $\rho$ has the following expression:

$$F_a = \frac{1}{2}\rho c_d A_v r_g^2 \omega^2. \tag{3.14}$$

The conventional service brake force on the wheel $F_{sb}$ is modeled using a static nonlinear function, a first order differential equation with a time constant $\tau_{sb}$, and a delay $\theta_{sb}$:

$$F_{sb} = f_{sb}(v_{sb}), \tag{3.15}$$

$$\frac{d}{dt}v_{sb}(t+\theta_{sb}) = \frac{1}{\tau_{sb}}(u_{sb} - v_{sb}(t+\theta_{sb})). \tag{3.16}$$

The static nonlinear function is a function of the applied pedal force, or simpler, the pedal displacement $u_{sb}$ (for details see [12],[23],[27]). The time constant and time delay $\tau_{sb}$ and $\theta_{sb}$, respectively, are nonlinear and uncertain functions of temperature and brake conditions.

It is well known that the service brakes have weak DC authority because of overheating. The current practice of "snubbing" the service brake (application of high pressure pulses) rather than "dragging" (application of a constant low pressure) exemplifies their low DC authority [11].

A block diagram of the vehicle model is shown in Figure 3.3

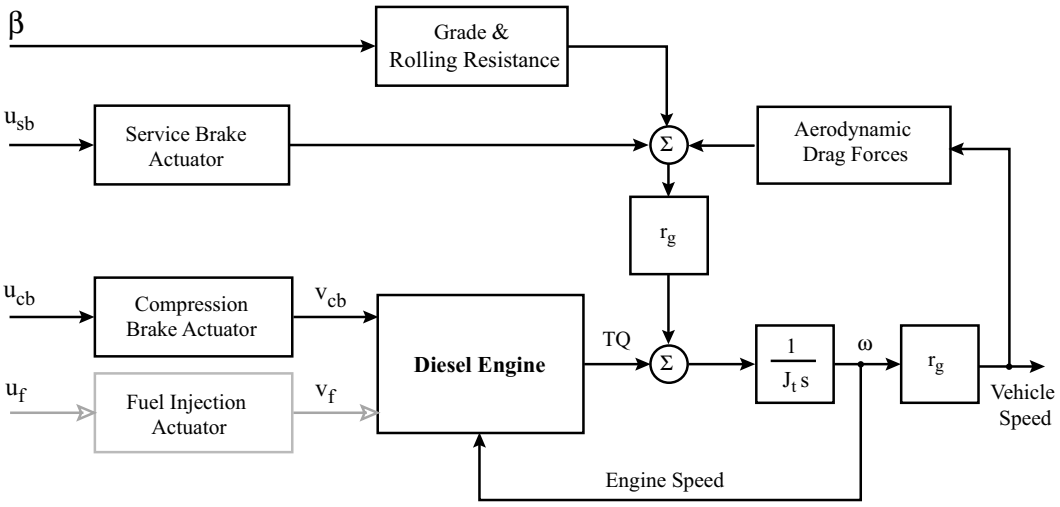


Figure 3.3: *Block diagram of the vehicle model.*

By rewriting (3.10) in terms of torque instead of forces we obtain the following vehicle model for *braking only:*

$$J_t(M, r_g)\dot{\omega} = TQ(v_{cb}, \omega) + TQ_\beta(\beta) - TQ_{sb}(v_{sb}) - TQ_a(\omega). \quad (3.17)$$

The compression brake torque identified in the previous section is denoted $TQ$, while $TQ_\beta$ denotes the torque due to road grade and rolling resistance. The torque due to the service brakes is given by $TQ_{sb}$, while $TQ_a$ represents the torque due to aerodynamic drag. The total vehicle inertia is given by $J_t$, and it is a function of mass $M$ and total gear ratio $r_g$.

Linearization of (3.17) at a nominal operating point, indicated by $|_0$, leads to the following expression:

$$\begin{aligned} J_t\Delta\omega &= \frac{\partial TQ}{\partial v_{cb}} \mid_0 \Delta v_{cb} + \frac{\partial TQ}{\partial \omega} \mid_0 \Delta\omega + \frac{\partial TQ_\beta}{\partial \beta} \mid_0 \Delta\beta \\ &\quad -\frac{\partial TQ_{sb}}{\partial v_{sb}} \mid_0 \Delta v_{sb} - \frac{\partial TQ_a}{\partial \omega}, \mid_0 \Delta\omega. \end{aligned} \quad (3.18)$$

The linearization of the compression brake torque $TQ$ consists of a static gain due to the linearization of (3.1) around nominal engine speed $\omega_0$:

$$\begin{aligned} k_\omega &= \frac{\partial TQ}{\partial \tilde{\omega}} \mid_0 \\ &= \alpha_1 + \alpha_3 W_{b0} + 2\alpha_4\omega_0 + 2\alpha_5 W_{b0}\omega_0, \end{aligned} \quad (3.19)$$

and a static gain given by the linearization around nominal brake valve timing $v_{cb0}$:

$$\begin{aligned} k_{W_b} &= \frac{\partial TQ}{\partial W_b} \mid_0 \\ &= \alpha_2 + \alpha_3\omega_0 + \alpha_5\omega_0^2. \end{aligned} \quad (3.20)$$

In addition to the gains, $TQ$ contains the the dynamics described in (3.2)–(3.8).

Laplace transformation of (3.18) results in following linear model for the vehicle dynamics:

$$\begin{aligned} J_t s\Delta\omega(s) &= G_{cb_v}(s)\Delta v_{cb}(s) + G_{cb_\omega}(s)\Delta\omega(s) + G_{sb_v}(s)\Delta v_{sb}(s) \\ &\quad G_\beta(s)\Delta\beta(s) + G_a(s)\Delta\omega(s). \end{aligned} \quad (3.21)$$

Grouping of terms, and closing the internal speed feedback-loop due to aerodynamic drag and compression brake engine speed dynamics, result in the following linear vehicle model for braking only:

$$\Delta\omega = G_v(s)[G_{cb}(s)\Delta v_{cb} + G_{sb}(s)\Delta v_{sb} + G_\beta(s)\Delta\beta], \quad (3.22)$$

where

$$G_v(s) = [J_t s - k_\omega \frac{c_\omega s + 1}{\tau_\omega s + 1} - (c_d A_v \omega_0 r_g^3)]^{-1}, \quad (3.23)$$

$$G_{cb}(s) = k_{W_b} \frac{cs + 1}{\tau s + 1}, \quad (3.24)$$

$$G_{sb}(s) = \frac{k_{sb} e^{-\theta_{sb} s}}{\tau_{sb} s + 1}, \quad (3.25)$$

$$G_\beta(s) = -r_g M g(\cos\beta_0 - f_r \sin\beta_0). \quad (3.26)$$

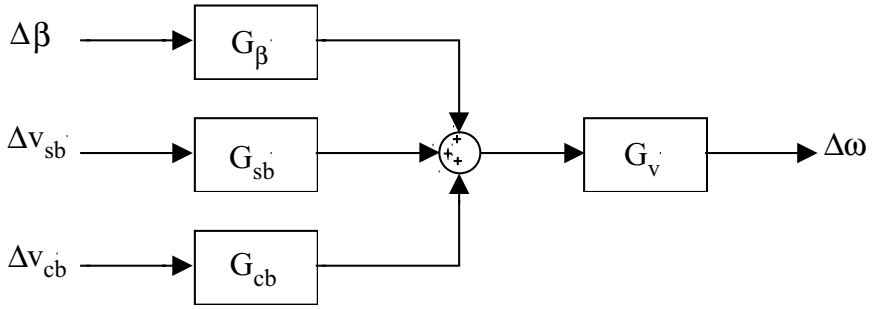


Figure 3.4: *Block diagram for linearized vehicle model for braking only.*

## 3.3 Sensitivity Analysis

In this section, we investigate how vehicle mass, road grade and gear selection affect the vehicle speed dynamic. A CHV is a vehicle system that can have various configurations. The total mass for the vehicle system can vary as much as 400 percent, from being a system of tractor alone, to being a system of tractor pulling fully loaded trailers. The CHV is also expected to encounter various downhill road grades, so an understanding of how this variable affects the vehicle speed is important. Moreover, the gear selection plays an important role, and has to be analyzed as well.

To quantify the effects mass $M$ and gear ratio $r_g$ have on the engine speed $\Delta\omega$ from $\Delta v_{cb}$, we analyze the transfer function given by (3.22)–(3.24):

$$\frac{\Delta\omega}{\Delta v_{cb}} = \frac{k_{W_b}(cs + 1)(\tau_\omega s + 1)}{(\tau s + 1)(\tau_g^2 s^2 + 2\zeta_g \tau_g s + 1)}, \quad (3.27)$$

where the time constant $\tau_g$ and damping factor $\zeta_g$ have the following form:

$$\tau_g = \left( \frac{(Mr_g^2 + I_e)\tau_\omega}{c_d A_v \omega_0 r_g^3 - k_\omega} \right)^{1/2} \tag{3.28}$$

$$\zeta_g = \frac{(c_d A_v \omega_0 r_g^3 - k_\omega)^{1/2}(Mr_g^2 + I_e) - k_\omega c_\omega + c_d A_v \omega_0 r_g^3}{2\left((Mr_g^2 + I_e)\tau_\omega\right)^{1/2}}. \tag{3.29}$$

From the pole-zero map in Figure 3.5 it is clear that the dominant pole corresponds to one of the roots in the quadratic part of the denominator of (3.27). We, therefore, continue by studying the sensitivity of the roots of the quadratic polynomial to changes in mass and gear ratio.

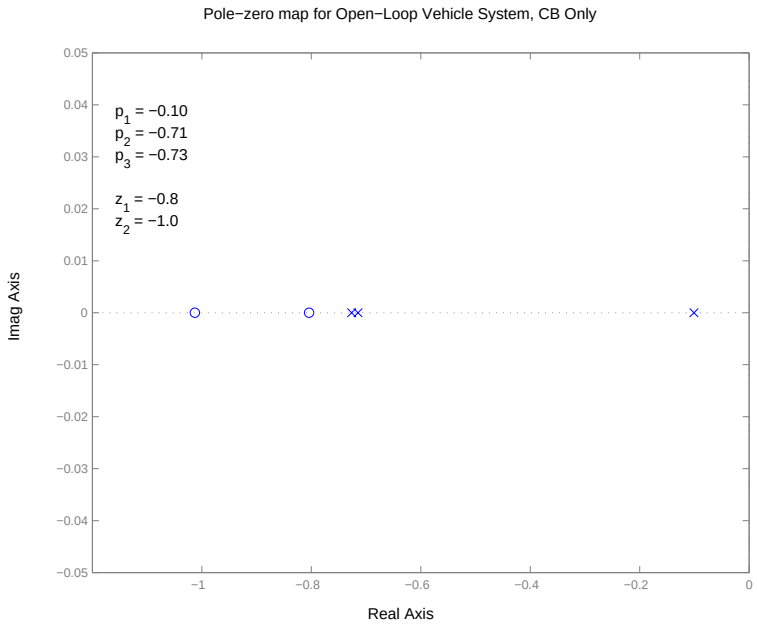


Figure 3.5: *Pole-zero map of the linearized compression brake model.*

The steady state gain for step changes in $\Delta v_{cb}$ is

$$\frac{\Delta\omega}{\Delta v_{cb}}(s=0) = \frac{k_{W_b}}{c_d A_v \omega_0 r_g^3 - k_\omega}. \tag{3.30}$$

Variations in mass do not affect the steady state speed of the vehicle but affect the transient behavior. Also, the gear ratio appears as a cubic term in the denominator. Small $r_g$ (corresponding to low gear numbers) results in high amplification, and, thus, higher steady state speed than higher gear selections. This is clearly evident in Figure 3.6.

A graphical representation of the engine speed's sensitivity to mass and gear changes, for a step input in brake valve timing, is shown in Figure 3.6. We show the engine speed time responses for three different vehicle masses and gear ratios for a unit step change in $\Delta v_{cb}$ from nominal brake valve timing $v_{cb0} = 640^o$. As

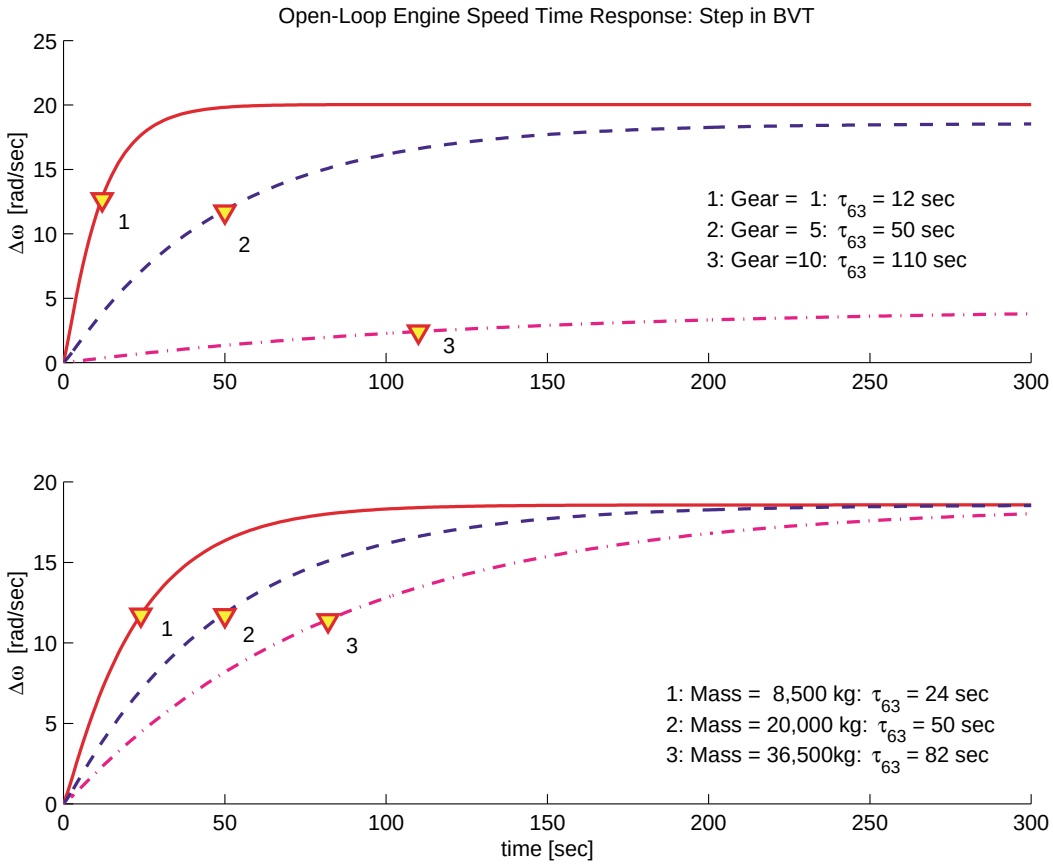


Figure 3.6: *Engine speed time response to step change in brake valve timing.*

expected, there is a significant sensitivity to changes in gear ratios, as seen in the upper plot in Figure 3.6. In fact, the time constant for the system varies from 12 seconds when using the first gear, to 110 seconds when using the tenth gear.

Variations in the vehicle mass also greatly influence the vehicle dynamics. The lower plot in Figure 3.6, shows that the time constant $\tau_{63}$, defined as the time at which the response is 63.2 % complete [24], increases from 24 seconds for tractor alone to 82 seconds for the combination of a tractor and fully loaded trailer(s).

To quantify the effect mass and gear ratios have on the engine speed dynamics due to step changes in the grade input $\Delta\beta$, we consider the following second order transfer function given by (3.22), (3.23) and (3.26):

$$\frac{\Delta\omega}{\Delta\beta} = \frac{-r_g Mg\left(\cos\beta_0 - f_r \sin\beta_0\right)}{(Mr_g^2 + I_e)\tau_\omega s^2 + \left((Mr_g^2 + I_e) - k_\omega c_\omega + c_d A_v \omega_0 r_g^3\right) s + \left(c_d A_v \omega_0 r_g^3 - k_\omega\right)}. \tag{3.31}$$

The steady state gain from $\Delta\beta$ to $\Delta\omega$ is given by

$$\frac{\Delta\omega}{\Delta\beta}(s=0) \;=\; \frac{-r_g Mg(\cos\beta_0 - f_r \sin\beta_0)}{c_d A_v \omega_0 r_g^3 - k_\omega}. \tag{3.32}$$

By examining the total gear ratio $r_g$ for all 10 gear numbers as shown in Figure 3.7, we find that for the nominal point we consider,

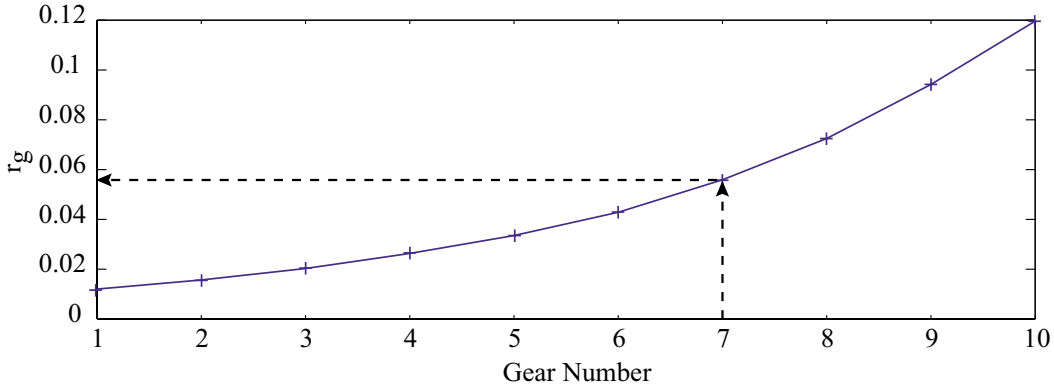


Figure 3.7: *Total gear ratio $r_g$ versus gear number selection.*

$$\omega_o = 157 \text{ and } k_\omega = -2.3,$$

for gear number 7 and smaller

$$k_\omega \gg \rho c_d A_v r_g^3 \omega_o.$$

This means that the aerodynamic drag dominates the denominator for larger gear numbers. The result is the following approximation of the steady-state gain:

$$\frac{\Delta\omega}{\Delta\beta} = \begin{cases} -\frac{M_g}{k_\omega} r_g & \text{for small gears (1–7)} \\ -\frac{M_g}{\rho c_d A_v \omega_o} \frac{1}{r_g^2} & \text{for large gears (8–10)} \end{cases}$$

It is, therefore, expected that the steady-state engine speed behaves in a non-monotonic way, as the gear number increases, which is clearly evident in the upper plot in Figure 3.8. The figure shows how much the engine speed dynamics, to a step change in grade $\Delta\beta = -0.06^o$ from nominal grade $\beta_0 = -3.4^o$, are affected by variations in mass and gear ratios.

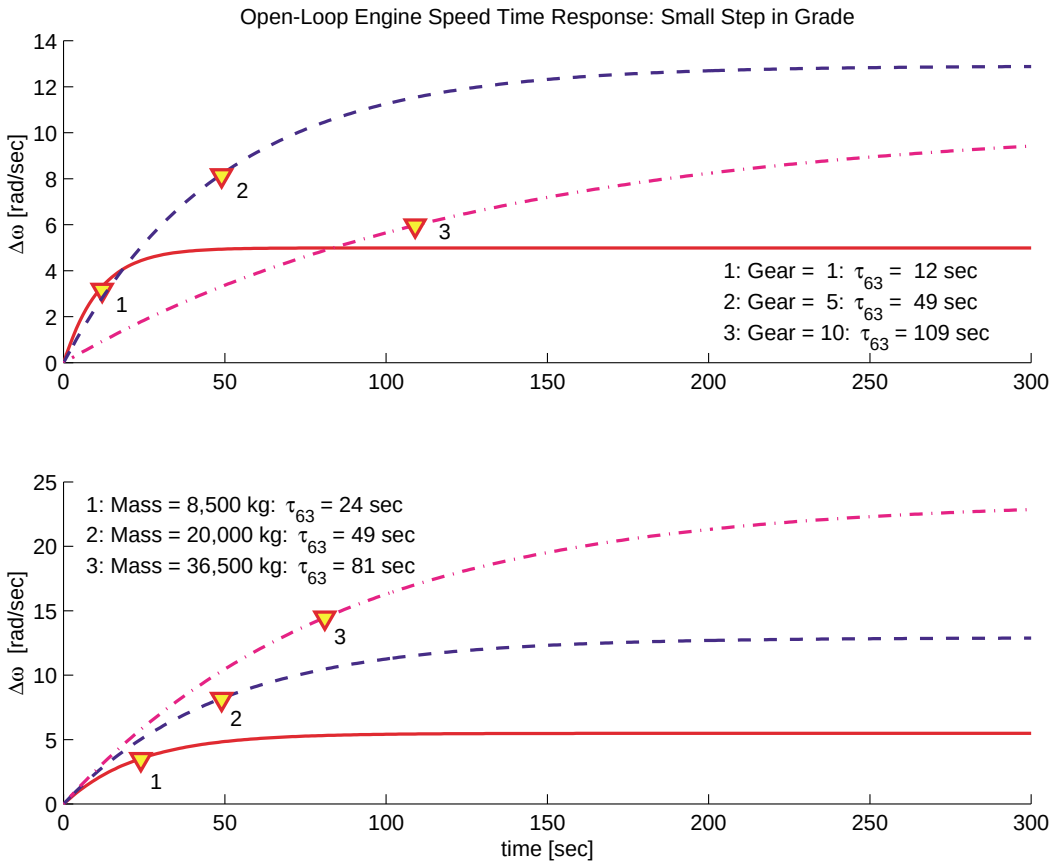


Figure 3.8: *Engine speed response to step change in grade.*

The time constant and the damping factor are given by (3.28) and (3.29), respectively. The time constant, $\tau_{63}$, varies from 12 to 109 seconds for gear one and ten, respectively, and show a monotonic behavior as expected. For variations in mass, as shown in the lower plot in Figure 3.8, the time constant varies from 24 seconds when the system consists of trailer alone, to 81 seconds for a system of tractor and fully loaded trailer(s).

Our sensitivity analysis indicates the need for a robust control design to address the CHV speed regulating and tracking problems during large parameter

deviations and unknown road conditions. This is pursued in Chapter4, where we in addition to a robust control design also summarize the work we have done using a model reference adaptive control (MRAC) approach.

## 3.4 Uncertainty Analysis

The linearized vehicle model (3.22) approximates the real vehicle system around one particular operating condition. As we already discussed in the previous section, the large variations in vehicle mass and road grade can significantly affect the longitudinal dynamics of heavy trucks. These parameter variations are the largest source of model uncertainties. In addition, there is another source of uncertainty due to the approximation we performed to derive the set of low-order models in Chapter 3.1. To handle these uncertainties, we derive in this section, uncertainty models needed for the robust control design carried out in Chapter 4.

By conducting a grid search between the minimum and maximum values for vehicle mass $M$, engine speed $\omega$, road grade $\beta$ and brake valve timing $v_{cb}$, as shown in Table 3.1 we compute the infinity norm of the transfer function between the disturbance input $\beta$ and the output $\omega$ for each set of parameters in the search.

| | | | |
|---|---|---|---|
| 15,000 | $\leq M \leq$ | 25,000 | (kg) |
| 105 | $\leq \omega \leq$ | 215 | (rad/sec) |
| -5 | $\leq \beta \leq$ | 0 | (deg) |
| 620 | $\leq v_{cb} \leq$ | 700 | (deg) |

Table 3.1: Range of vehicle parameters.

We refer to the set of parameters that results in the lowest peak (over the frequency range), relative to the peaks for the other sets of parameters, as the "best" vehicle configuration. The road grade $\beta$ has the lowest authority to affect the engine speed $\omega$ for this particular set of parameters. The parameter set corresponding to the highest peak of the magnitude of the transfer function between $\beta$ and $\omega$, on the other hand, is referred to as the "worst." Finally, based on the "best" and "worst" sets of parameters we derive the parameter set that we refer to as "nominal" vehicle configuration. The set of parameters for all

these vehicle configurations are specified in Table 3.2.

| Parameter: | Nominal | Best | Worst | Unit |
|---|---|---|---|---|
| $M$ | 20,000 | 15,000 | 25,000 | kg |
| $\omega$ | 157 | 215 | 105 | rad/sec |
| $\beta$ | -3.43 | -5.0 | 0 | deg |
| $v_{cb}$ | 640 | 700 | 620 | deg |

Table 3.2: Vehicle configuration parameters.

### 3.4.1 Modeling of Uncertainties

For each transfer function (3.23)-(3.26) of the linearized vehicle model (3.22) we specify the uncertainty models as multiplicative perturbations in the following form [26]:

$$\Pi : G_p(s) \quad = \quad G_0(s)(1 + W\Delta_I)$$

where $\Pi$ is the set of possible perturbed system models, $G_p \in \Pi$ is the particular perturbed system model, $G_0 \in \Pi$ is the nominal system model with no uncertainty, $\Delta_I$ is any stable proper transfer function such that $||\Delta_I(j\omega)||_{\inf} \leq 1$, and $W$ is perturbation weight. Specifically, the perturbation weight $W$ can be derived as a stable and rational transfer function that covers the maximum magnitude for the relative errors between the nominal model $G_0$ and $G_p$ for the possible range of parameter variations, i.e.

$$l_I(\omega) \quad = \quad \max_{G_p \in \Pi} |\frac{G_p(j\omega) - G_0(j\omega)}{G_0(j\omega)}|. \tag{3.33}$$

Following the procedure (3.33) we now derive the perturbation weights $W_1$, $W_2$, $W_3$, and $W_4$ for the transfer functions $G_{cb}(s)$, $G_v(s)$, $G_\beta(s)$ and $G_{sb}(s)$, respectively, as is shown next.

To obtain the uncertainty weight $W_1$, corresponding to the the compression brake actuator dynamics model (3.24), we first specify the nominal transfer function $G_{cb0}(s)$. Since the coefficients $c$, $\tau$ and $k_{W_B}$ in (3.24) are the functions of engine speed $\omega$, we have the following numerical values of these parameters for the nominal, best and worse vehicle configurations:

| Parameter: | Nominal Condition | Best Condition | Worst Condition |
|---|---|---|---|
| $c$ | 1.0 | 0.6 | 2.6 |
| $\tau$ | 1.4 | 0.9 | 3.5 |
| $k_{W_B}$ | 8.1 | 14 | 3.4 |

Therefore, the nominal model for (3.24) is given by the following transfer function:

$$G_{cb0} = 8.1\frac{s+1}{1.4s+1}. \tag{3.34}$$

We next plot the relative errors

$$l_1(\omega) \;=\; \frac{G_{cb}(j\omega) - G_{cb0}(j\omega)}{G_{cb0}(j\omega)}, \tag{3.35}$$

for the range of parameter variations $\Pi$ as specified in Table 3.1. A stable and rational transfer function that covers the maximum magnitude for $l_1(\omega)$ is given by the following uncertainty weight:

$$W_1 \;=\; \frac{0.5613s^3 + 4.11s^2 + 11.23s + 4.398}{s^3 + 5.982s^2 + 12.7s + 6.976}, \tag{3.36}$$

and is shown in Figure 3.9.

Analogously, we next obtain the uncertainty weight $W_2$, corresponding to the transfer function $G_v(s)$ of the vehicle part of the system (3.23). Specifically, a stable rational transfer function that covers the range of relative errors (from the nominal) is

$$G_{v0} = \frac{0.0396s + 0.0318}{s^2 + 0.8271s + 0.0732},$$

and $G_v$ for range of parameters specified in Table 3.1, is given by:

$$W_2 \;=\; \frac{0.2839s^3 + 4.682s^2 + 13.28s + 6.053}{s^3 + 14.35s^2 + 21.63s + 7.864}. \tag{3.37}$$

and is shown in Figure 3.10.

The nominal transfer function for grade disturbance $C_{\beta 0}$ is modeled as a static gain with numerical values corresponding to nominal, best and worst case are $-6565$, $-4914$ and $-8218$, respectively. The uncertainty weight $W_3$ then has the following value:

$$W_3 \;=\; 0.2501. \tag{3.38}$$

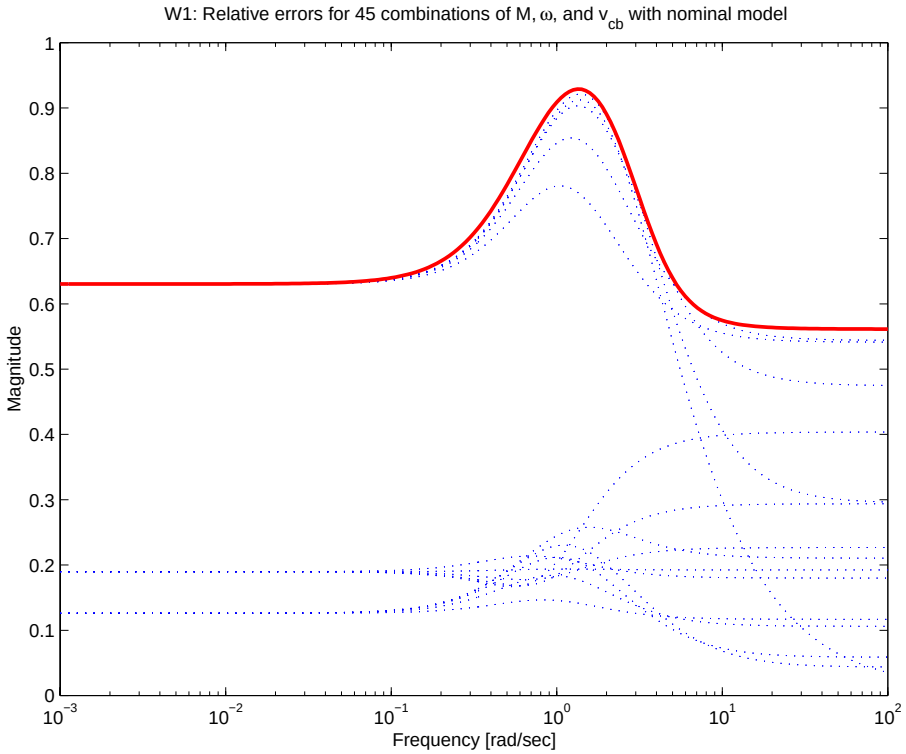
W1: Relative errors for 45 combinations of M, ω, and v_cb with nominal model
Magnitude
Frequency [rad/sec]
0
0.1
0.2
0.3
0.4
0.5
0.6
0.7
0.8
0.9
1
10^-3
10^-2
10^-1
10^0
10^1
10^2

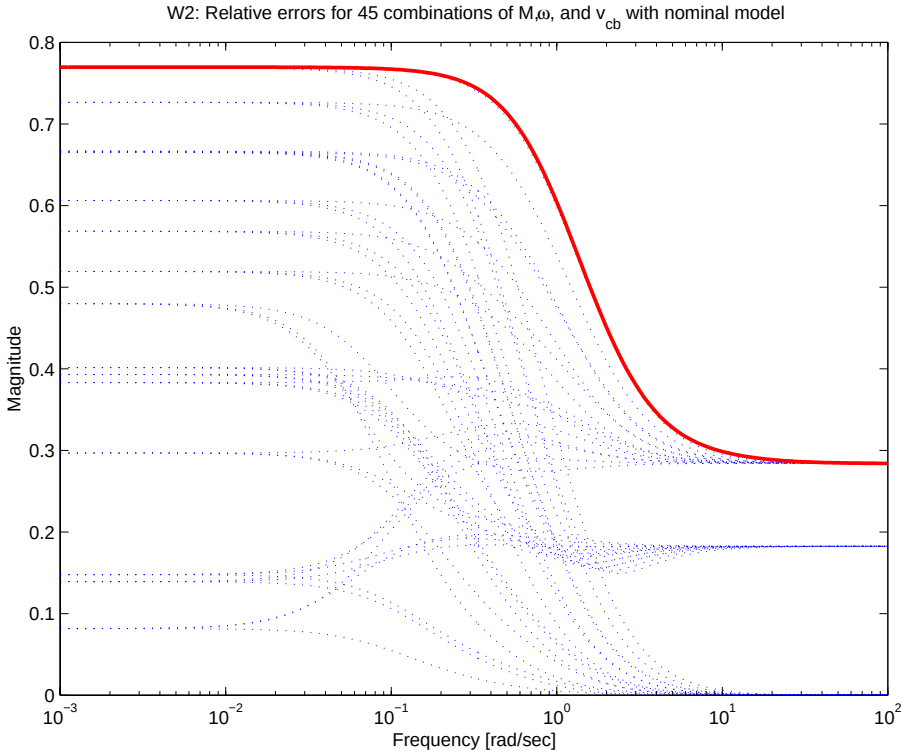
W2: Relative errors for 45 combinations of M,ω, and v_cb with nominal model
Magnitude
Frequency [rad/sec]
0
0.1
0.2
0.3
0.4
0.5
0.6
0.7
0.8
10^-3
10^-2
10^-1
10^0
10^1
10^2

Unlike the other parts of the vehicle model, the parameters of the transfer function for service brakes dynamics, $G_{sb}$ from (3.25), do not depend on the vehicle configuration parameters specified in Table 3.2. We, therefore, choose a delay free nominal model, and consider the relative errors between that one and the "real" models when the nominal parameter values for $K_{sb}$, $\theta_{sb}$, and $\tau_{sb}$ in (3.25) are subjected to 50 percent error. A rational transfer that covers the set of relative errors between the chosen nominal model and perturbed models is given by the following transfer function:

$$W_4 = \frac{0.5(0.69s^2 + 1.66s + 1)}{0.04s^2 + 0.4s + 1} \tag{3.39}$$

# Chapter 4

# Control Design

In this chapter we design controllers employing classical and modern control techniques, for the vehicle system developed in the previous chapters. Specifically, an initial design of two PI-controllers is carried out under the assumption that the vehicle system may be approximated by a gain and a first order lag. Initial linear simulations along with the analysis carried out in Chapter 3.3 indicate that better performance is achieved using robust and nonlinear controllers. Using the concept of structured singular values, we design a $12th$ order $H_\infty$ controller and a $20th$ order $\mu$–controller using DK iterations. In addition, we summarize work we have done within MOU 393 on a model reference adaptive controller design. Through extensive simulations, using the $24th$ order nonlinear vehicle model, we demonstrate the performance of the controllers.

## 4.1 Classical Linear Control Design

In this section, we employ a classical Proportional plus Integral (PI) controller design to regulate the vehicle speed $v(t)$ to the desired constant vehicle speed $v_c$, during a long descent down a grade. Since the engine rotational speed $\omega$, is related to the vehicle speed by $v = \omega r_g$, this ensures that $\omega \to \omega_c$ as long as the gear $r_g$ is constant. Additionally, we assume that the braking with the compression brake is preferable, because we want to minimize the use of service brakes to potentially reduce the wear of the friction pads in the brakes.

From the open-loop pole-zero map of the vehicle given in Figure 3.5 we know that there is a slow dominant pole at $p_1 = -0.1$. As an crude approximation of

the open-loop vehicle system for compression braking only we, therefore, use the following first order transfer function for this initial PI–control design:

$$G_x \;=\; \frac{-\frac{k_{W_b}}{k_\omega}}{\frac{1}{p_1}s+1}. \tag{4.1}$$

A practical control design approach is to specify the closed-loop transfer function to achieve a realistic settling time for the vehicle system [24]. For a Class-8 CHV, a realistic settling time to a step change in brake valve timing $v_{cb}$ is approximately 7 seconds, whereas the desirable engine speed excursion away from nominal value is $\Delta\omega \leq 5$ rad/sec.

We design a PI–controller $G_c$ such that the closed-loop control system shown in Figure 4.1 satisfies the following expression:

$$\frac{G_c G_x}{1+G_c G_x} = \frac{1}{\tau_{des}\, s+1} \tag{4.2}$$

Solving for $G_c$ gives

$$G_c = \frac{1}{G_x}\frac{1}{\tau_{des}\, s}.$$

Using $G_x$ from (4.1), the controller $G_c$ has the following form:

$$G_c(s) = -\frac{k_{W_b}}{k_\omega}\frac{\frac{1}{p_1}s+1}{\tau_{des}\, s} \tag{4.3}$$

To conform to the form of a standard PI-controller where

$$G_{PI}(s) = k_p\left(\frac{\tau_I\, s+1}{\tau_I\, s}\right), \tag{4.4}$$

we set $\tau_{des} = 1/p_1$. We refer to this initial PI-controller as $G_{PI1}$ and we select nominal values for its parameters as

$$kp = -\frac{k_{W_b}}{k_\omega} = 0.3 \quad \text{and} \quad \tau_I = \tau_{des} = 10 \text{ seconds}$$

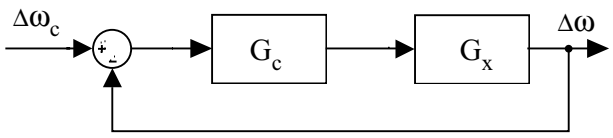


Figure 4.1: *Block diagram for compression braking only feedback control system.*

The performance for the closed loop control system is demonstrated using the linearized model given in (3.23). Specifically, a step change in engine speed $\Delta\omega_{ref}$ = -10 rad/sec from nominal $\omega_0 = 157$ rad/sec is shown in the left column in Figure 4.2, whereas the performance for a step in grade $\Delta\beta = -2^o$ away from nominal $\beta_0 = -3.4^o$ is shown in the right column. Clearly, the performance is

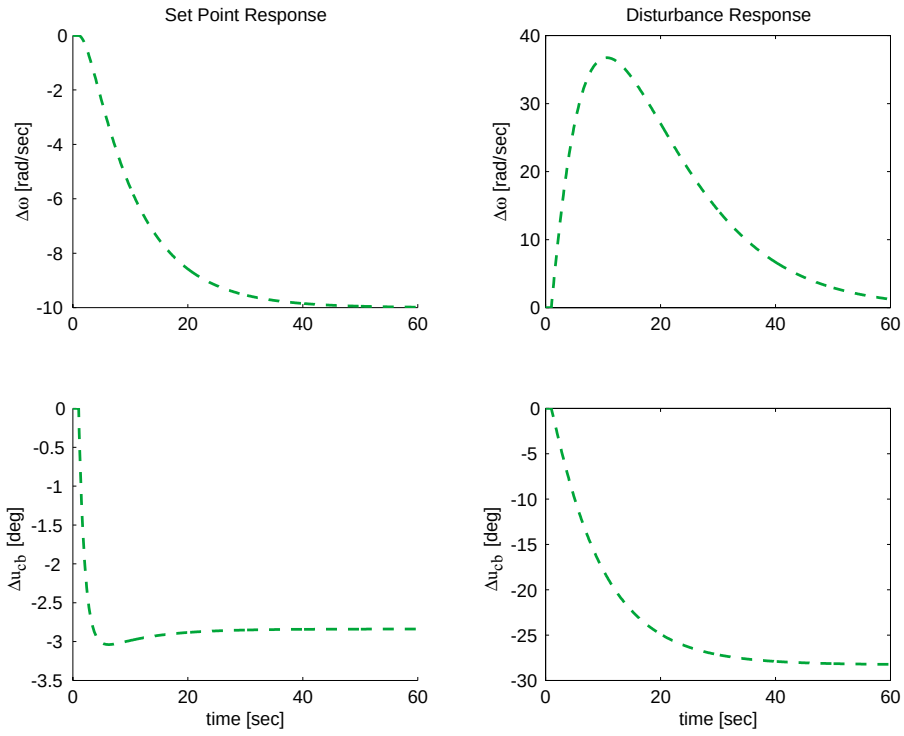


Figure 4.2: *The closed-loop vehicle performance for step changes in engine speed and road grade using the controller* $G_{PI1}$.

not as good as we want it to be, the settling time is approximately 30 seconds whereas the engine excursion due to a step change in grade is approximately 37 rad/sec.

The first step in improving the controller performance is to increase the gain from 0.3 to 10, while keeping the integral time constant at 10 seconds. We denote the controller with this set of parameters $G_{PI2}$ and show the performance for the same step changes in engine speed and road grade in Figure 4.3. To reduce the overshoot for a step in grade further, we reduce the integral time from 10 to 5 seconds while increasing the gain from 0.3 to 5. We refer to this PI-controller $PI_{nom}$ as the *nominal* one, as its performance will be used as a benchmark for

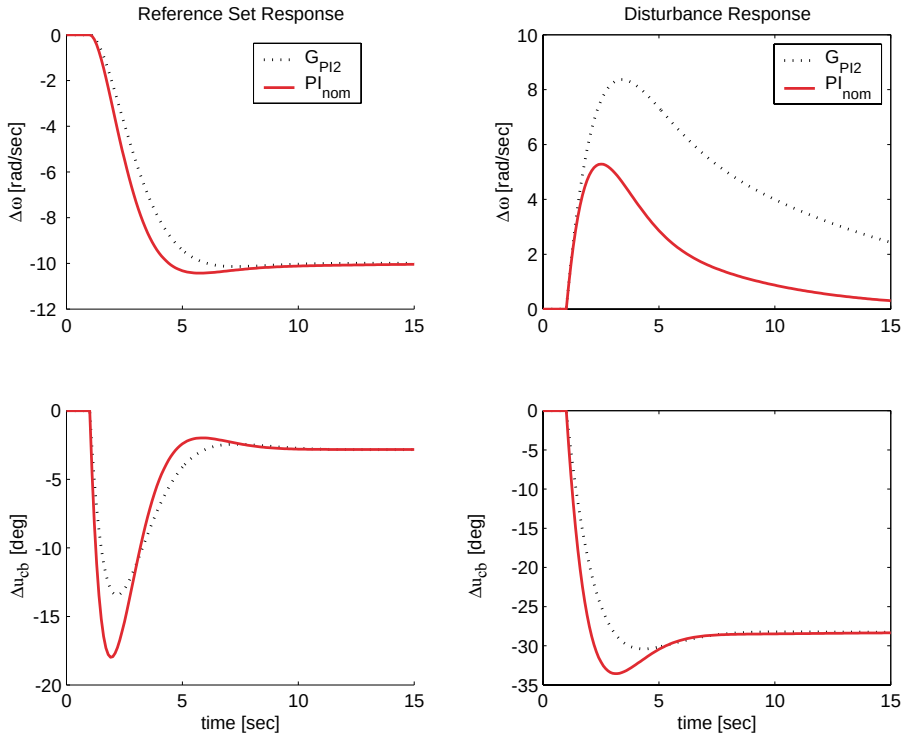


Figure 4.3: *The closed-loop vehicle performance for step changes in engine speed and road grade using two different PI–controllers.*

the other controller designs. The performance of $PI_{nom}$ is shown as a solid line in Figure 4.3.

For clarity, the various controller gains are given in Table 4.1.

| Controller Setting | $G_{PI1}$ | $G_{PI2}$ | $PI_{nom}$ |
|---|---|---|---|
| $k_p$ | 0.3 | 3 | 5 |
| $\tau_I$ | 10 | 10 | 5 |

Table 4.1: Standard PI-controller parameters.

## 4.2 Modern Linear Robust Control Design

In this section, we employ modern linear robust control design and analysis methodologies to the problem of speed control. The nominal PI-controller designed in the previous section is designed using a single nominal operating point.

However, from the he sensitivity analysis carried out in Chapter 3.3 it is clear that we are dealing with a set of vehicle models due to parameter variations described in Chapter 3.4.

A control system is, in general, said to be robust if it is insensitive to differences between the actual physical plant and the model used for the control design, and robustness is typically evaluated by robust stability (RS) and robust performance (RP) criteria. If a closed-loop system remains stable for all plants within the specified set of plants, then it is regarded as being robustly stable. Robust performance, on the other hand, is determined by how well the set of plants meet the specified control objectives.

The control objective is speed control and regulation, hence we want to both minimize steady state error between desired and measured speed and to minimize the effect of various disturbances at low and mid-frequency range. This objective can be reflected in the following choice of performance weight $W_p$ on the engine speed output (engine speed deviation from the reference):

$$W_p = \frac{10(0.01s+1)}{33.3s+1} \tag{4.5}$$

To penalize excessive control effort and mitigate the effects of actuator saturation, we employ the following weight on the variable compression brake control signal:

$$W_c = \frac{0.04(1/26s+1)}{1/500s+1} \tag{4.6}$$

The brake valve opening happens once per cylinder per engine cycle, hence, the maximum useful bandwidth for the actuator corresponds to one engine cycle. However, to reduce the actuator effort, we use a bandwidth corresponding to three engine cycles.

Moreover, in a real vehicle application the speed measurement will be noisy. To be able to handle this, we include the following weight on the noise:

$$W_n = \frac{0.25s+60}{s+3000} \tag{4.7}$$

The frequency responses for the performance weights are shown in Figure 4.4.

### 4.2.1 Robustness Analysis

Figure 4.5 shows the block diagram for the vehicle system where all the uncertainties have bee modeled as multiplicative perturbations, since this is often the preferred perturbation form [26]. By manipulating Figure 4.5 into Figure 4.6, we have a general framework for conducting robust control synthesis and analysis of the vehicle system. In the left half of Figure 4.6, the open-loop vehicle system is referred to as plant $P$, and contains the nominal transfer functions, the uncertainty weights, and the performance weights. The $\Delta$ block in the upper part of the figure contains the uncertain elements. The controller is denoted $K$. The signals shown in the figure are: the control signal $\Delta u_{cb}$, the road grade $\Delta\beta$, the noise $\Delta n$, the engine speed output $\Delta\omega$, the design weight output for the control actuator $\Delta o_c$, and the design weight output for engine speed $\Delta o_p$. In addition, $iw_\Delta$ and $ow_\Delta$ are the input and output vectors of the uncertainty block $\Delta$.

By performing a lower Linear Fractional Transformation (LFT) of $P$ and $K$, in the left half of the figure, we arrive at the closed-loop system $N$, which is used for robustness analysis, for any given controller $K$ [26].

$$N = F_l(P, K) = P_{11} + P_{12}K(I - P_{22}K)^{-1}P_{21}. \tag{4.8}$$

Similarly, by performing an upper LFT, we arrive at a closed–loop system $F$, where

$$F = F_u(N, \Delta) = N_{22} + N_{21}\Delta(I - N_{11}\Delta)^{-1}N_{12}. \tag{4.9}$$

Based on Figure 4.6, and (4.8) and (4.9), we summarize the requirements for nominal and robust stability, and nominal and robust performance as follows:

- **Nominal Stability (NS):**$N$ is internally stable; i.e. for given $K$, the closed–loop system is stable for the nominal plant $P$.
- **Nominal Performance (NP):** NS and $\|N_{22}\|_\infty < 1$.
- **Robust Stability (RS):** NS, F is stable, and $\forall\Delta$, $\|\Delta\|_\infty \leq 1$; i.e. for given $K$, the closed–loop system remains stable for all plants in the specified uncertainty set.
- **Robust Performance (RP):** NS and $\|F\|_\infty < 1$, and $\forall\Delta$, $\|\Delta\|_\infty \leq 1$.

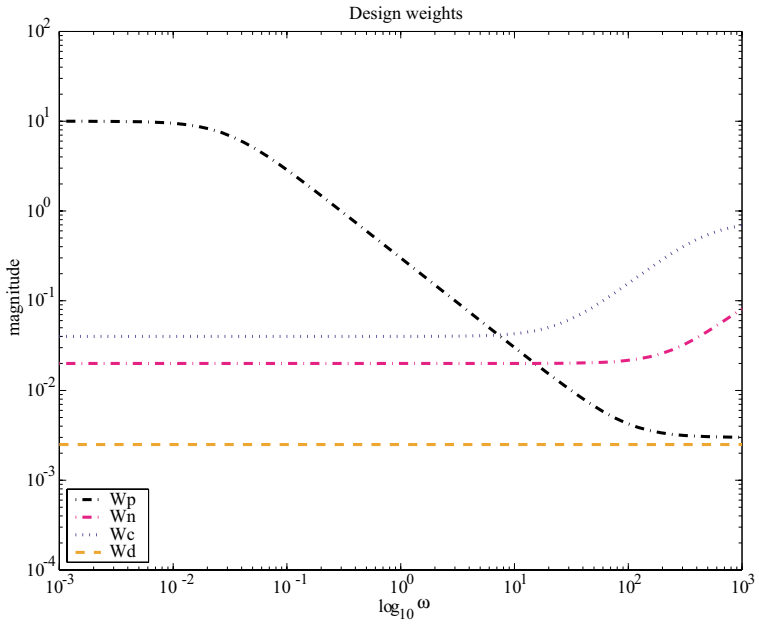


Figure 4.4: *Frequency response for the performance weights.*

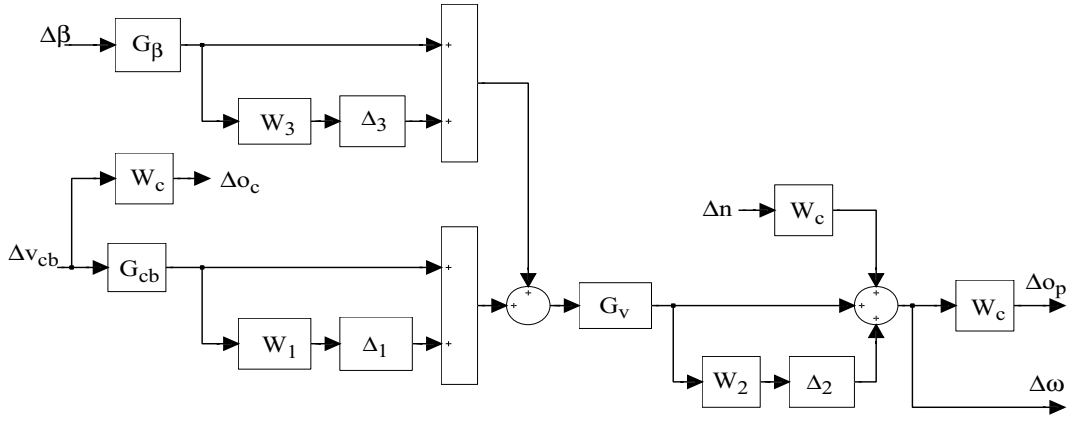


Figure 4.5: *Block diagram of the vehicle system where all the uncertainties are modeled as multiplicative perturbations.*

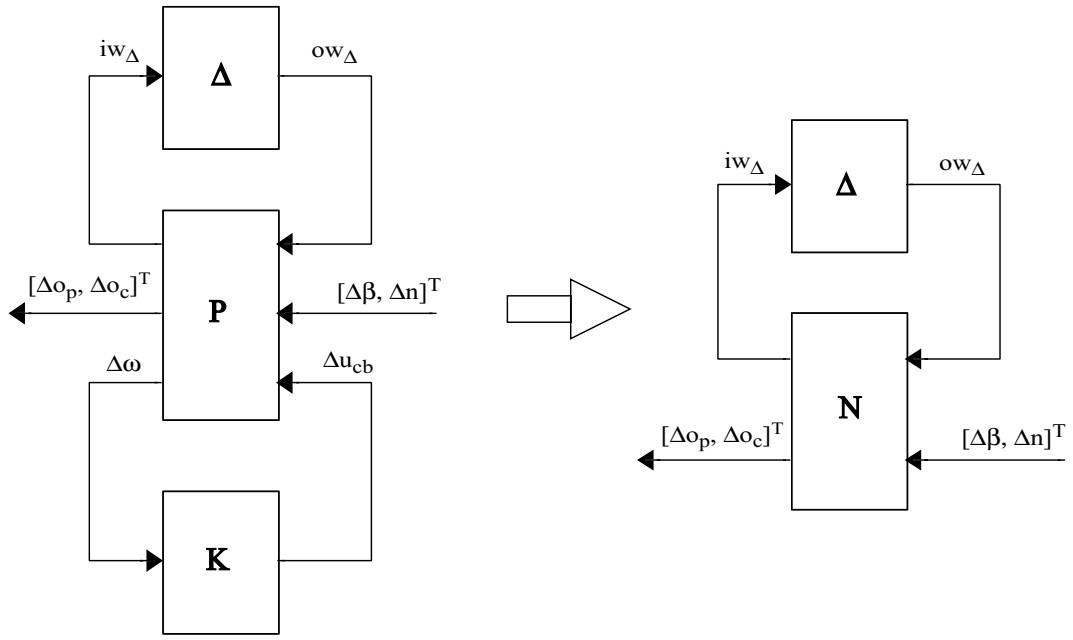


Figure 4.6: ***Left:*** *General configuration for robust control synthesis.* ***Right:*** *General configuration for robust analysis.*

A practical way of determining NS, NP, RS, and RP is to calculate the structured singular value $\mu$. The positive, real valued function $\mu_\Delta(M)$ is defined on a complex valued matrix $M$ the following way [26]:

$$\mu_\Delta(M) = \frac{1}{min(k_m \mid det(I - k_m M\Delta) = 0 \text{for structured } \Delta, \overline{\sigma}(\Delta) \leq 1)} \quad (4.10)$$

If no such structured $\Delta$ exists, then $\mu_\Delta(M) = 0$.

This means that if $\mu$=1, then there exists a perturbation $\Delta$ with $\overline{\sigma}(\Delta) = 1$ which is large enough to make $(I - M\Delta)$ singular. Therefore, the requirements for NP, RS and RP are satisfied if $\mu < 1$ in each case.

### 4.2.2 Robust PI–Controller

By reducing the integral time $\tau_I$ from 5 to 1 second, while keeping $k_p = 5$ constant, we are able to achieve NP, RS, and RP using a single PI-controller, as we see from the three $\mu$ plots in Figure 4.7. Also seen in the same figure is that the only robustness requirement the nominal PI–controller fails to meet is robust performance. The robust PI–controller, on the other hand satisfies all

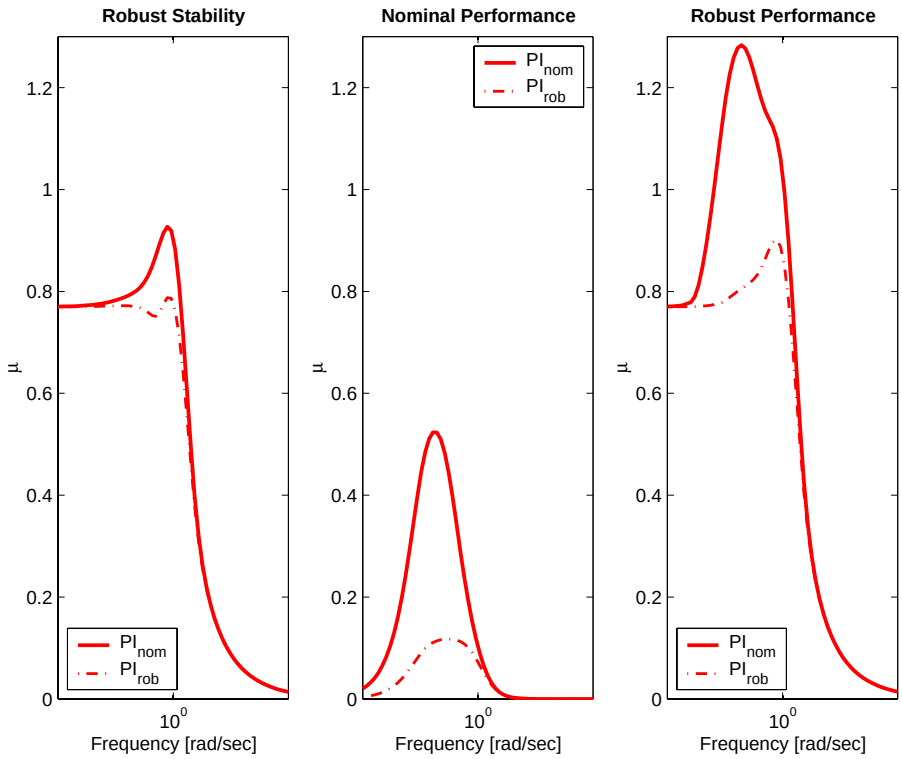


Figure 4.7: *$\mu$-analysis for $PI_{nom}$ and $PI_{rob}$.*

three requirements, but as seen in Figure 4.8, the oscillatory time response of the this controller is not satisfactory. We use this as a motivation to design a $H_\infty$–controller.

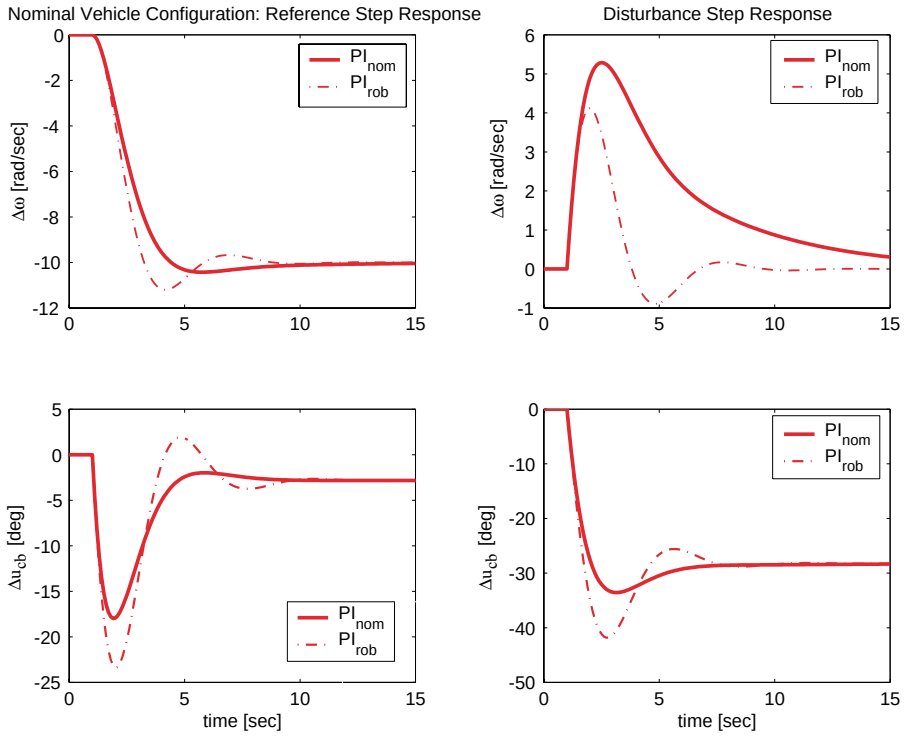


Figure 4.8: *Reference and disturbance responses for the nominal and the robust PI-controllers, simulated using the linearized vehicle model.*

### 4.2.3 $H_\infty$– Controller

We design a $H_\infty$-controller for the nominal vehicle plant shown in Figure 4.6. Specifically, we consider $\gamma(K)$ that minimizes the closed–loop $H_\infty$-norm between all our inputs and outputs for a given $K$:

$$\gamma(K)_{opt} = \| N \|_\infty = \| F_l(P,K) \|_\infty \ . \tag{4.11}$$

In practice, however, it is easier to design a sub-optimal controller, where the assumption is that given a $\gamma > \gamma_{opt}$, find all stabilizing controllers $K$ such that

$$\| F_l(P,K) \|_\infty < \gamma. \tag{4.12}$$

For the actual synthesis, we used the *hinfsys* command in Matlab.

The performance for a step change in engine speed $\Delta\omega_{ref}$ = -10 rad/sec from nominal $\omega_0 = 157$ rad/sec is shown in the left column in Figure 4.9, whereas the performance for a step in grade $\Delta\beta = -2^o$ from nominal $\beta_0 = -3.4^o$ is shown in the right column.

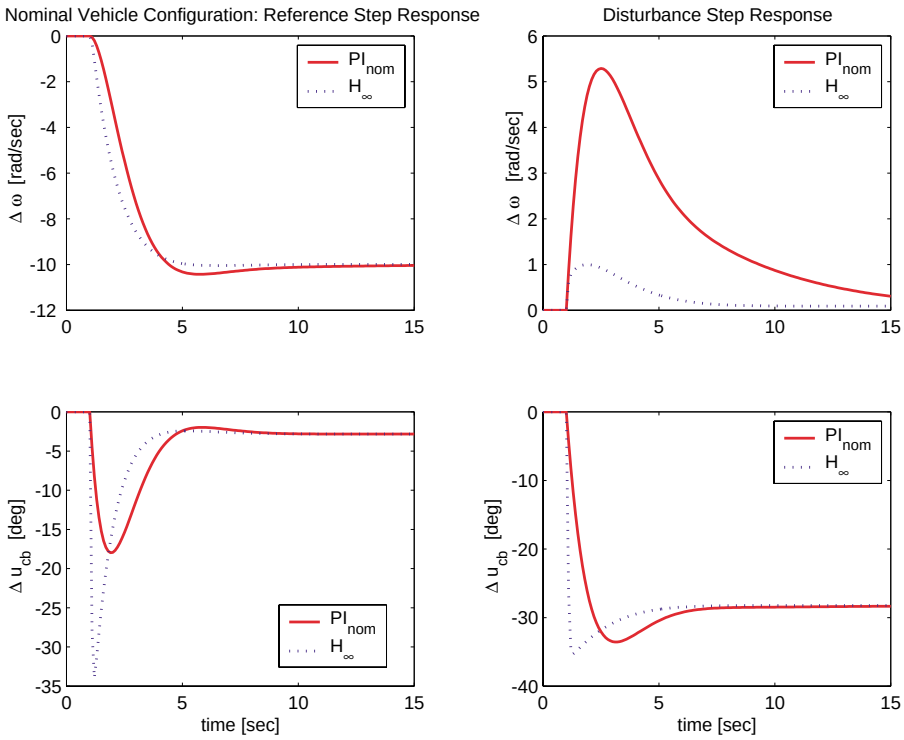


Figure 4.9: *Reference and disturbance responses for the $H_\infty$–controller.*

The resulting $\mu$–analysis for the closed–loop vehicle system is shown in Figure 4.10. As seen in this figure, the peak values for both RS and RP are greater than one for the $H_\infty$–controller (dotted line), implying that this nominal design is not able to satisfy robust stability and robust performance. We, therefore, proceed with a $\mu$–optimal control design scheme, using the $D$–$K$ iteration approach to satisfy all three robustness criteria.

### 4.2.4 D–K Iteration Approach

Since the constrains on $\mu$ were not satisfied by the nominal $H_\infty$–controller, we employ the $D$–$K$ iteration approach. This is an approach that uses an approx-

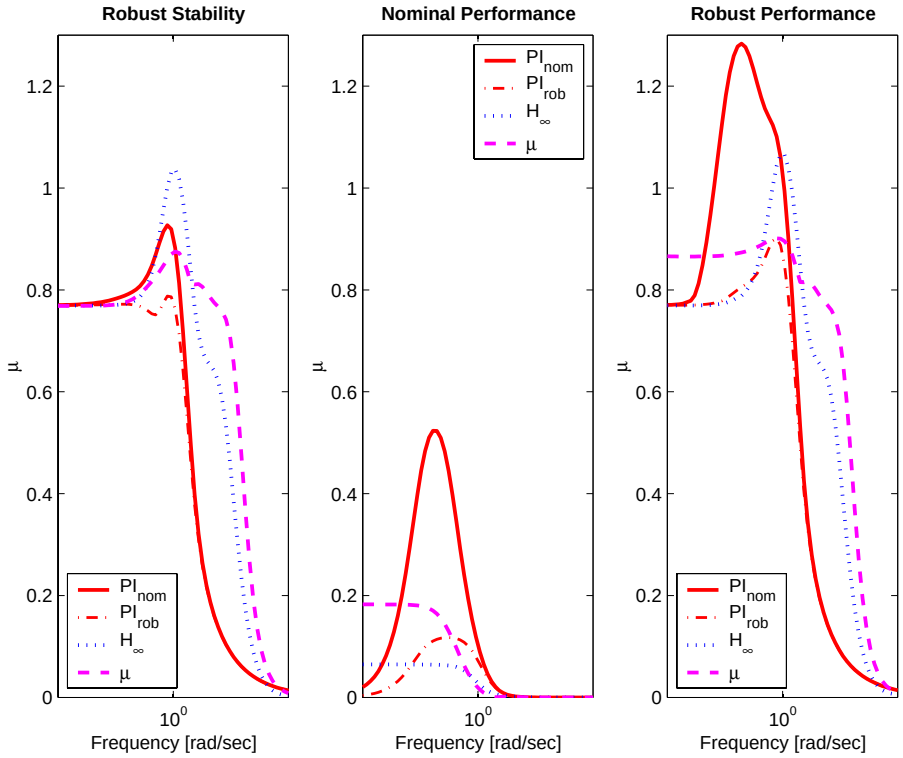


Figure 4.10: *$\mu$-analysis for all four controllers.*

imate procedure to minimize the peak value of $\mu$ for the closed–loop system $F_l(P, K)$. The resulting controller is a $\mu$–optimal controller. For the actual synthesis we used the graphical user interface *dkitgui* in Matlab. In Table 4.2 we summarize the essential information from each iteration.

| Iteration Summary | | | | |
|---|---|---|---|---|
| Iteration no. | 1 | 2 | 3 | 4 |
| Controller order | 0 | 8 | 8 | 10 |
| Total D-scale order | 12 | 20 | 20 | 22 |
| Gamma achieved | 11.60 | 2.17 | 1.16 | 0.95 |
| Peak $\mu$-value | 5.40 | 1.80 | 1.14 | 0.91 |

Table 4.2: Summary of the $D$–$K$ iteration approach.

The performance for a step change in reference input and a step change in grade is shown in Figure 4.11. The performance of the $\mu$–controller is significantly better than for the nominal PI–controller. The speed excursion is negli-

gible for disturbance step response shown in the left column of Figure 4.11. The

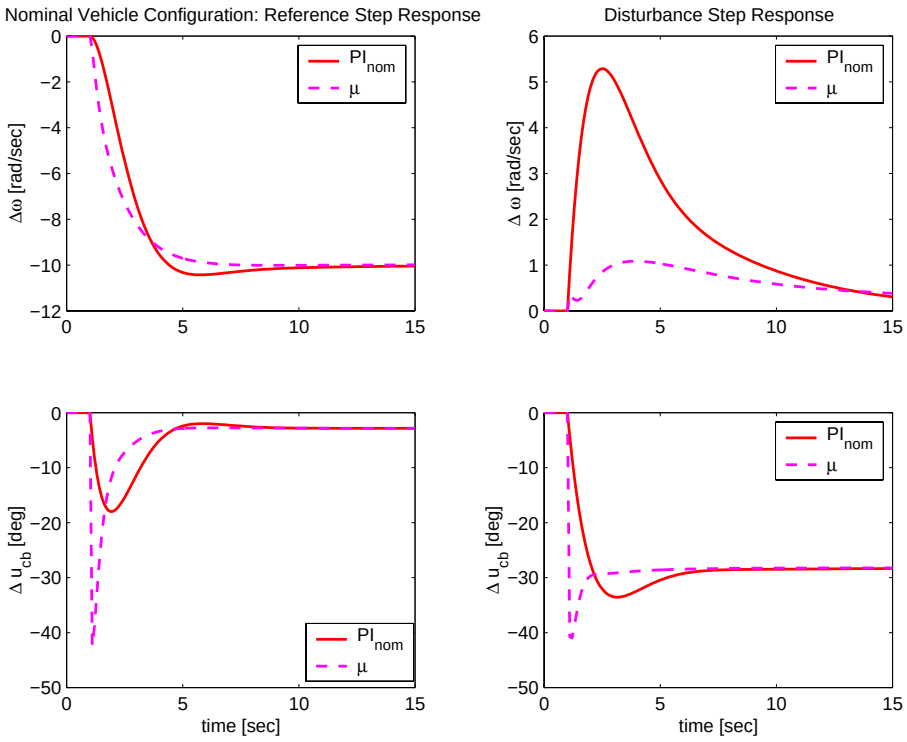


Figure 4.11: *Reference and disturbance time responses for the $\mu$–controller.*

three robustness criteria are satisfied as shown in Figure 4.10, but the controller order is high. After balanced realization and model order truncation we are able to bring down the controller order from 22 to 20, but when it comes to physical implementation, such a high-order controller might be impractical.

## 4.3 Comparative Linear Simulations

To compare the performance for each of the linear control designs, we show in Figure 4.12 reference and disturbance responses for the nominal vehicle configuration. As expected, the nominal PI–controller is the one that allows the highest speed excursion for a disturbance step response. The $H_\infty$ and the $\mu$–controllers both have negligible speed excursion for disturbance step responses, and their control efforts are also reasonably close to the two PI–controllers. For the reference step responses in the left column of Figure 4.12, on the other hand, all four controllers perform similar. The robust PI–controller is the most oscillatory (as

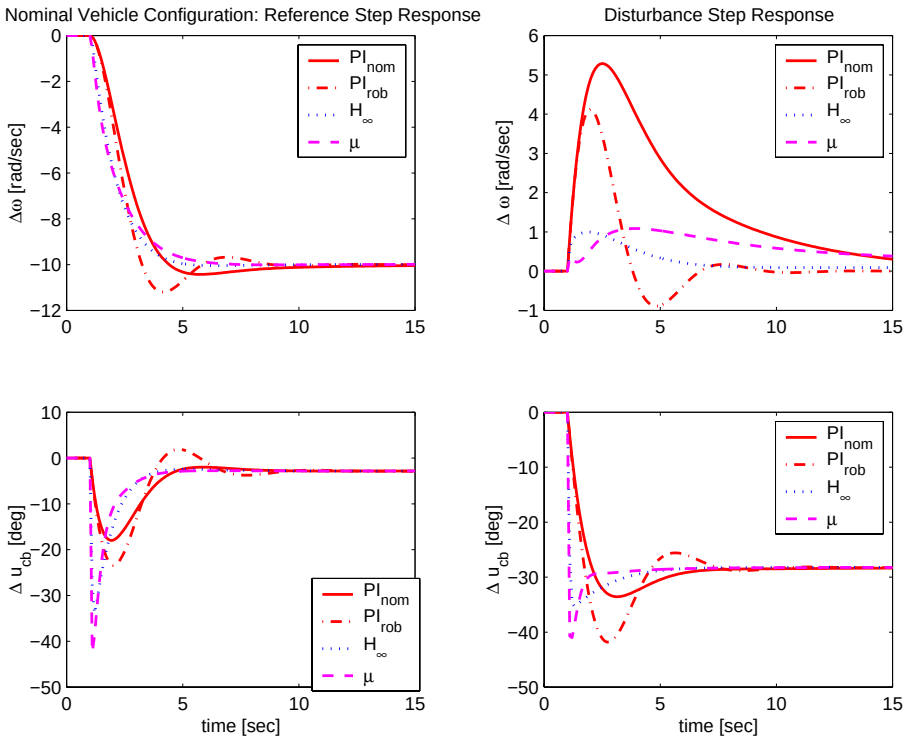


Figure 4.12: ***Nominal Vehicle Configuration:*** *Reference and disturbance time responses for all four controllers.*

expected) and the the $\mu$–controller which has the highest model order is using the most control effort to track the speed reference.

In Figure 4.13, on the other hand, we demonstrate the performance for the worst vehicle configuration. Qualitatively, the controller performances are similar to the ones for the nominal vehicle configuration. The differences between the four controllers are more noticeable in this figure as compared to Figure 4.12. This is expected since we are testing the controllers at their design limits.

The frequency responses for each of the controllers are shown in Figure 4.14. One interesting observation here is the difference between the nominal and the robust PI–controllers frequency responses. The reduction of the integral time for the nominal PI–controller leads to the robust one which exhibits oscillatory behavior. The reason for this is that when we increase the slope of the gain, from solid to dash-dotted lines in Figure 4.14, we increase, at the same time, the cross–over frequency. Disturbances are, therefore, attenuated less by the robust PI–controller than by the nominal one, resulting in the oscillatory behavior seen

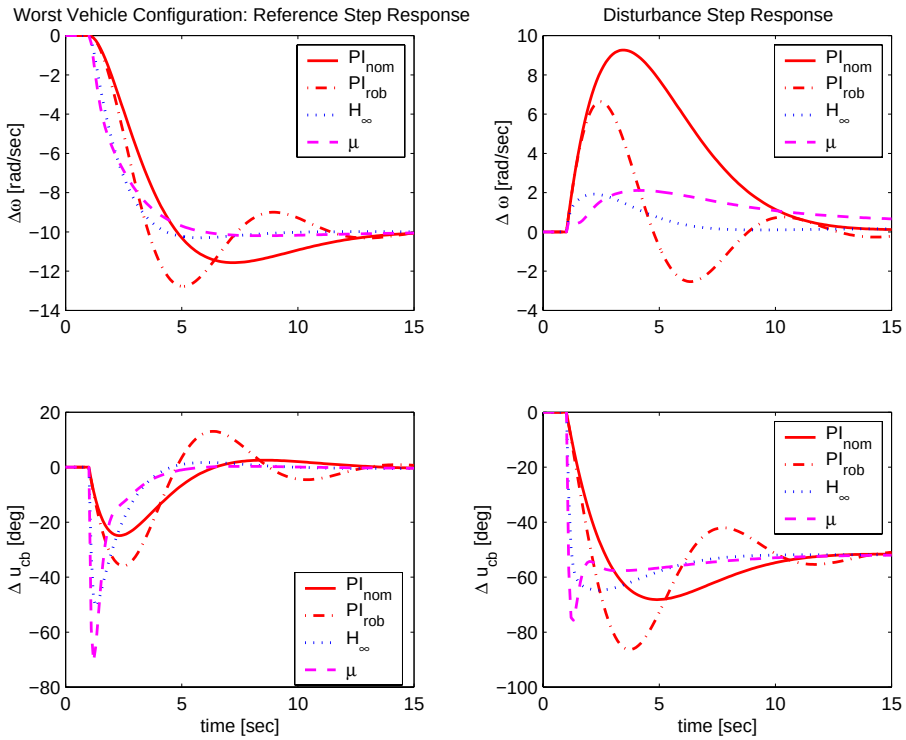


Figure 4.13: ***Worst Vehicle Configuration:*** *Reference and disturbance time responses for all four controllers.*

in Figures 4.12, and 4.13.

## 4.4 Nonlinear Control Design

In this section, we summarize the model reference adaptive control (MRAC) design presented in [9]. The assumption here is that vehicle mass is constant but unknown, and that the gear ratio $r_g$ remains fixed, which means that the total vehicle inertia $J_t$ is an unknown constant. In addition, we assume that the road grade $\beta$ is unknown.

Parameterizing the vehicle model in 3.10, we get:

$$\dot{\omega} = \frac{1}{\theta_1}(T_{cb} - r_g^3 C_q \omega^2 + \theta_2) \tag{4.13}$$

$$\dot{T}_{cb} = -\lambda_{cb}(T_{cb} - T_{st}), \tag{4.14}$$

where $T_{st}$ is now considered as a control input, and $\theta_1$, $\theta_2$ are the unknown

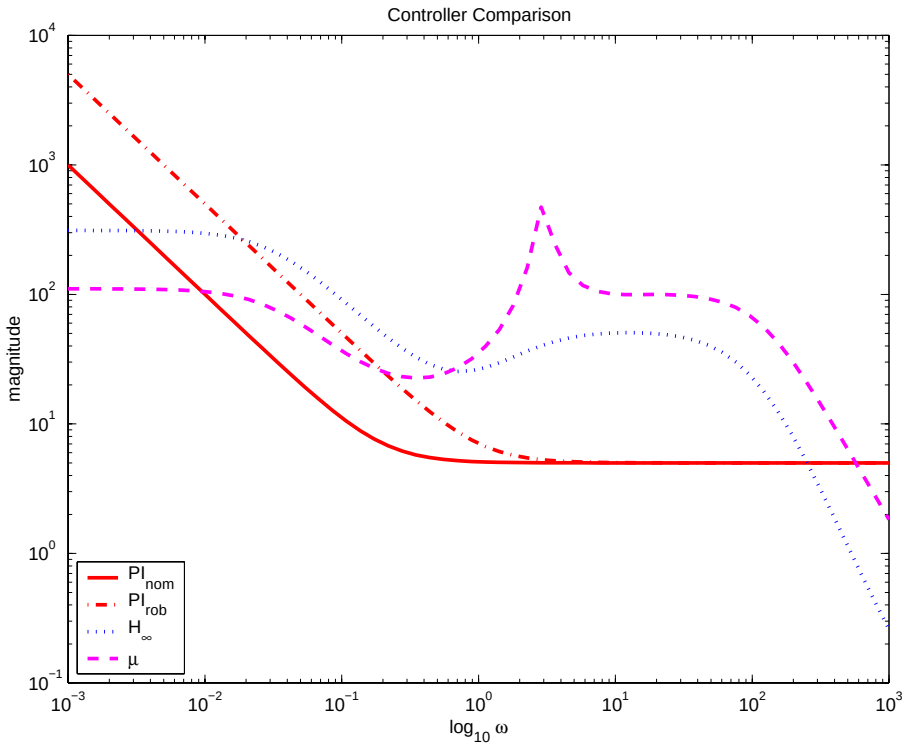


Figure 4.14: *Bode plots for all four controllers.*

parameters,

$$\theta_1 = J_t > 0, \ \theta_2 = r_g F_\beta.$$

The controller is designed using a backstepping approach [19]. In accordance with this iterative design procedure we first design a stabilizing control law $u(e, \hat{\theta}_1, \hat{\theta}_2)$ for (4.13), treating $T_{cb}$ as a *virtual* input to the first-order system.

To design the MRAC we introduce a reference model that captures the desired closed-loop behavior. Specifically,

$$\dot{\omega}_{ref} = -\lambda\omega_{ref} + \lambda\omega_c, \tag{4.15}$$

where $\omega_c(t)$ is the desired vehicle speed and $\lambda > 0$ controls the speed of response.

Denoting the tracking error by $e = \omega - \omega_{ref}$, we obtain:

$$\dot{e} = \frac{1}{\theta_1}(u - r_g^3 C_q \omega^2 + \theta_2) + \lambda\omega_{ref} - \lambda\omega_c. \tag{4.16}$$

Using the certainty equivalence principle, we define the feedback law as fol-

lows:

$$u = r_g^3 C_q \omega^2 - \theta_2 - \theta_1 \lambda(\omega - \omega_c). \tag{4.17}$$

If $\theta_1$, $\theta_2$ were known, this controller would guarantee that $e(t) = \omega(t) - \omega_{ref}(t) \to 0$. Since the parameters are unknown, we replace them by their estimates:

$$u = r_g^3 C_q \omega^2 - \hat{\theta}_2 - \hat{\theta}_1 \lambda(\omega - \omega_c). \tag{4.18}$$

The parameters $\hat{\theta}_1$, $\hat{\theta}_2$ is adjusted by using the following speed gradient based adaptation law:

$$\dot{\hat{\theta}}_1 = \gamma_1 e \lambda(\omega - \omega_c),\ \gamma_1 > 0. \tag{4.19}$$

$$\dot{\hat{\theta}}_2 = \gamma_2 e,\ \gamma_2 > 0. \tag{4.20}$$

We augment the controller in (4.19)-(4.20) with a projection scheme that ensures that the parameter estimates are bounded within a realistic feasible range. The parameter updates are stopped if $\hat{\theta}_1$, $\hat{\theta}_2$ attempt to leave their respective feasible intervals:

$$\dot{\hat{\theta}}_1 = Proj_1[\gamma_1 e \lambda(\omega - \omega_c), \hat{\theta}_1], \tag{4.21}$$

$$\dot{\hat{\theta}}_2 = Proj_2[\gamma_2 e, \hat{\theta}_2], . \tag{4.22}$$

As shown in (see [9]), this projection scheme improves the parameter estimate transient behavior as well.

Recall that $T_{cb}$ is not the real control input, therefore, in accordance with the backstepping design procedure we denote the error between $T_{cb}$ and the real control input $u$ by $z = T_{cb} - u(e, \hat{\theta}_1, \hat{\theta}_2)$. To account for this error, we use the following Lyapunov function to prove convergence $e(t) \to 0$ (for details see [9]):

$$V(e, z, \tilde{\theta}_1, \tilde{\theta}_2) = \frac{1}{2}e^2 + \frac{1}{2\gamma_1}\tilde{\theta}_1^2 + \frac{1}{2\gamma_2}\tilde{\theta}_2^2 + \frac{1}{2}z^2 \geq 0. \tag{4.23}$$

Since we know that $z = T_{cb} - u$, we show in ([9]) that

$$T_{st} = (1 - k\lambda_{cb}^{-1})T_{cb} - \lambda_{cb}^{-1}\left(e - ku - \dot{u}\right), k > 0. \tag{4.24}$$

guarantees that $\dot{V} \leq 0$.

To avoid having to measure acceleration directly to make the controller implementable, we approximate the derivative of speed with a dirty derivative as

suggested in [19]. This results in the following model reference adaptive controller:

$$\begin{aligned} T_{st} &= (1 - k\lambda_{cb}^{-1})T_{cb} - \lambda_{cb}^{-1}\left(e - ku - \hat{\dot{u}}\right) \\ u &= r_g^3 C_q \omega^2 - \hat{\theta}_2 - \hat{\theta}_1 \lambda(\omega - \omega_c), \\ \hat{\dot{u}} &= (2C_q r_g^3 \omega - \hat{\theta}_1 \lambda)\dot{\omega}_f - \lambda(\omega - \omega_c)\dot{\hat{\theta}}_1 - \dot{\hat{\theta}}_2 + \hat{\theta}_1 \lambda \dot{\omega}_c \\ \dot{\omega}_f &= \tau(\omega - \omega_f), \\ \dot{\hat{\theta}}_1 &= Proj_1[\gamma_1 e \lambda(\omega - \omega_c), \hat{\theta}_1], \\ \dot{\hat{\theta}}_2 &= Proj_2[\gamma_2 e, \hat{\theta}_2]. \end{aligned} \tag{4.25}$$

In addition to avoiding acceleration measurements, we avoid measuring the shaft torque $T_{cb}$ by using an open-loop observer,

$$\dot{\hat{T}}_{cb} = -\lambda_{cb}(\hat{T}_{cb} - T_{st}).$$

The estimate $\hat{T}_{cb}$ replaces $T_{cb}$ in the control law (4.24). The solution of $\dot{e}_{cb} = -\lambda_{cb} e_{cb}$, where $e_{cb} = \hat{T}_{cb} - T_{cb}$ exponentially converges to zero, hence we verify in [9] that the algorithm properties are preserved with this observer. Additionally, we show that parameter convergence is achieved under persistence of excitation type of conditions for a reduced order model.

In Figure 4.15 we show the MRAC's speed tracking performance, and mass and grade estimation properties. Although we do not achieve convergence of the estimates due to the highly nonlinear vehicle model, the speed tracking, which is the prime objective, is very good.

## 4.5 Simulations on Full Order Model

To compare the performance of the various controllers, we simulate the corresponding closed-loop system using the $24^{th}$ order, nonlinear vehicle model developed in [20]-[22]. Needless to say, closing the loop with a $12^{th}$ order $H_\infty$–controller and with a $20^{th}$ order $\mu$–controller is computational very heavy. For the $\mu$–controller, the ratio between computation time and simulation time for the nominal speed tracking is approximately 50:1; i.e. simulating the full order, closed–loop vehicle system for 70 seconds take approximately 60 minutes on a 1 GHz computer equipped with 512 MB RAM.

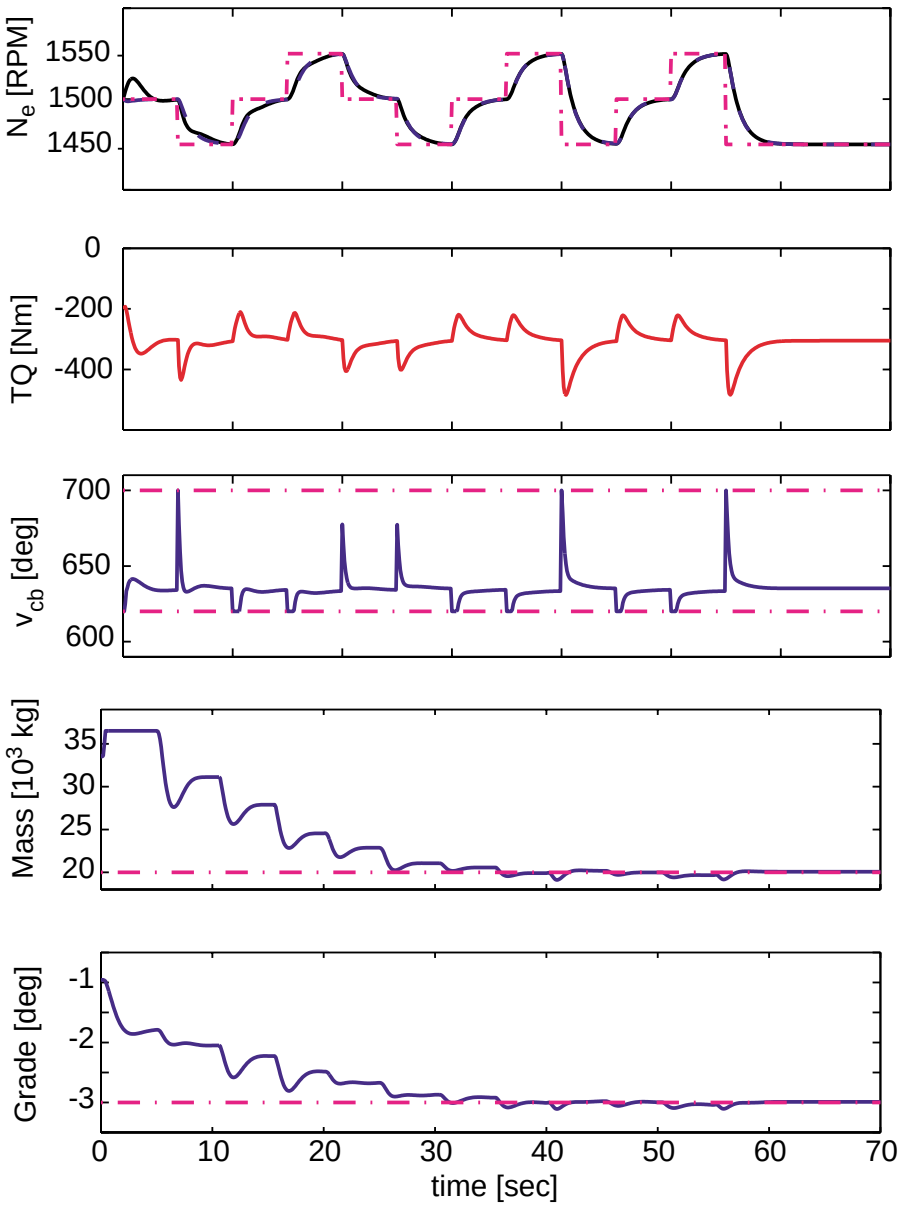


Figure 4.15: *MRAC's speed tracking performance.*

In the following Figures 4.17 – 4.20 we demonstrate speed tracking and disturbance rejection performances for all the controllers.

### 4.5.1 Simulation Implementation

To implement the linear controllers in the full nonlinear vehicle model, we have to add a nominal value $W_{b0}$ to the control output $\Delta u_{cb}$ in (4.4) to ensure that $\Delta u_{cb} = 0$ results in a steady-state response for any chosen operating point. Figure 4.16 shows a block diagram for the nonlinear vehicle system, where the controller is implemented the following way:

$$u_{cb}(t) = \Delta u_{cb}(t) + W_{b0}.$$

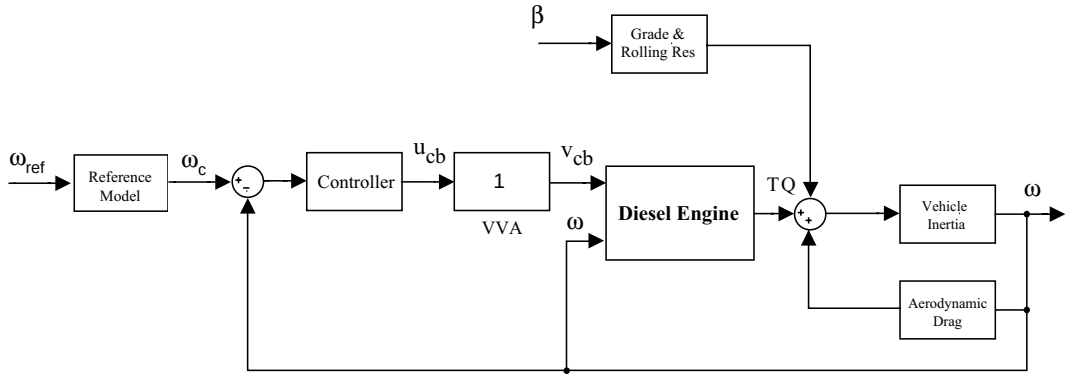


Figure 4.16: *Block diagram for full nonlinear vehicle model.*

### 4.5.2 Speed Tracking:

To compare the two PI-controllers, the $H_\infty$ and the $\mu$–controllers with the MRAC, we use the same reference model (4.15) for all our simulations. This means that the commanded reference signal $\omega_c$ is filtered through (4.15), resulting in $\omega_{ref}$ which is the signal the controllers are tracking.

In Figure 4.17, we compare the speed tracking performance for the nominal vehicle configuration, where the engine speed profile is show in the upper plot, the control signal $u_{cb}$ in the middle, while the averaged engine torque is shown in the lower plot.

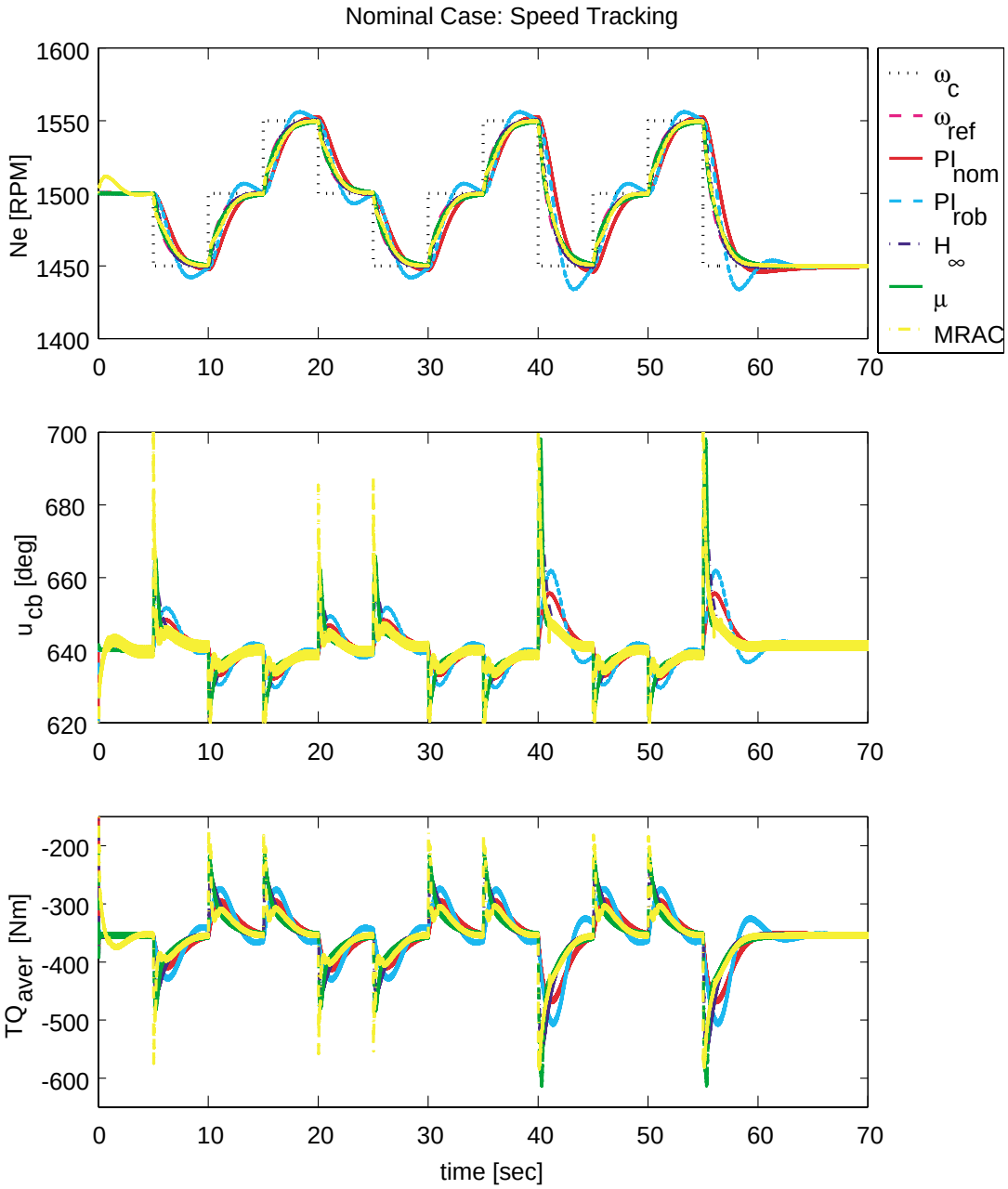


Figure 4.17: ***Nominal Vehicle Configuration:*** *Comparison of the speed reference tracking performances for all the controllers implemented on the full order nonlinear vehicle model.*

All the controllers are able to track the speed profile. Showing the details in the time scale in Figure 4.18, we note that MRAC is using the most control effort (middle plot) to follow the speed profile perfectly. Using a little less control effort, both the $H_\infty$ and the $\mu$–controllers are demonstrating perfect tracking as well. Also evident in the same figure is that the robust PI–controller $PI_{rob}$, has the most overshoot, and that the nominal PI–controller $PI_{nom}$, has the slowest response.

### 4.5.3 Disturbance Rejection

To demonstrate the disturbance rejection performance for the controllers, we simulate a step change in grade $\Delta\beta = -2^o$ from nominal value $\beta = -3.4^o$, at time $t = 1$ second. This is shown in Figure 4.19 for the nominal vehicle configuration. The control objective here is speed regulation, and the controller that does the poorest job in terms of speed deviation is the nominal PI–controller, $PI_{nom}$. The $H_\infty$ and the $\mu$–controllers perform extremely well compared to $PI_{nom}$ and $PI_{rob}$, at the cost of increased use of control effort $u_{cb}$ as evident in the middle plot in Figure 4.19.

In all the simulation we have presented so far, the true value of mass and grade are assumed known. This, however, is not the case for the MRAC, which is evident in the first second of the simulation in Figure 4.19. Here, the initial conditions for mass and grade are assumed to be off by 50 % compared to the true values defined as the nominal vehicle configuration in Table 3.2.

To further demonstrate the disturbance rejection properties of the five controllers, we once again simulate the same step change in road grade, but this time we use the worst vehicle configuration. The result of this simulation is shown in Figure 4.20. Again, a very erratic behavior due to operating close to the switching point between combustion and compression braking is evident in the middle and the lower plot. Similarly to the simulation results using the nominal vehicle configuration, both PI–controllers speed trajectories deviate more away from desired speed, than the higher-order controllers. However, they do not have the same erratic behavior problem as the The $H_\infty$ and the $\mu$–controllers do.

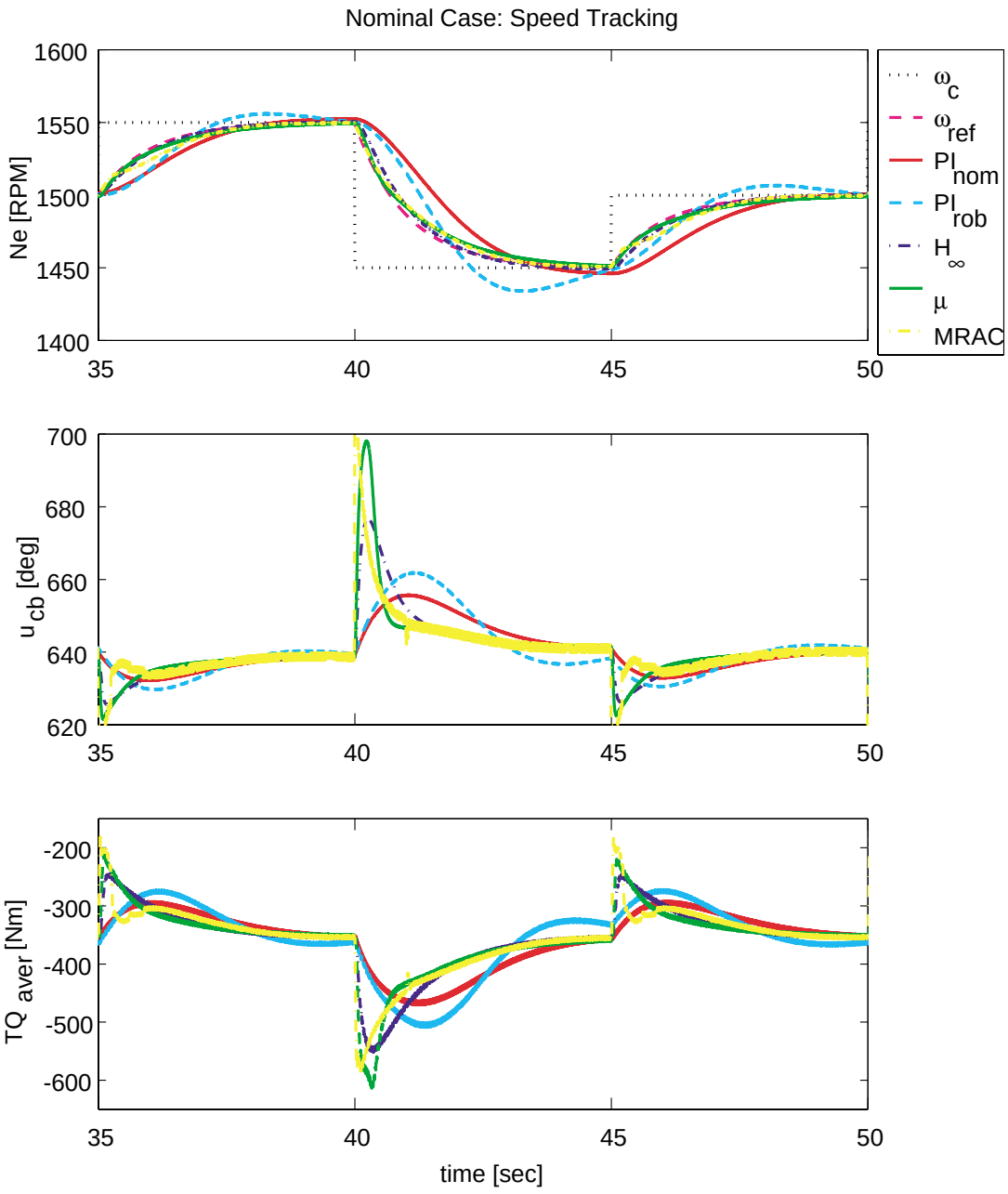


Figure 4.18: ***Nominal Vehicle Configuration:*** *Speed reference tracking for all the controllers, here shown in details on the time scale.*

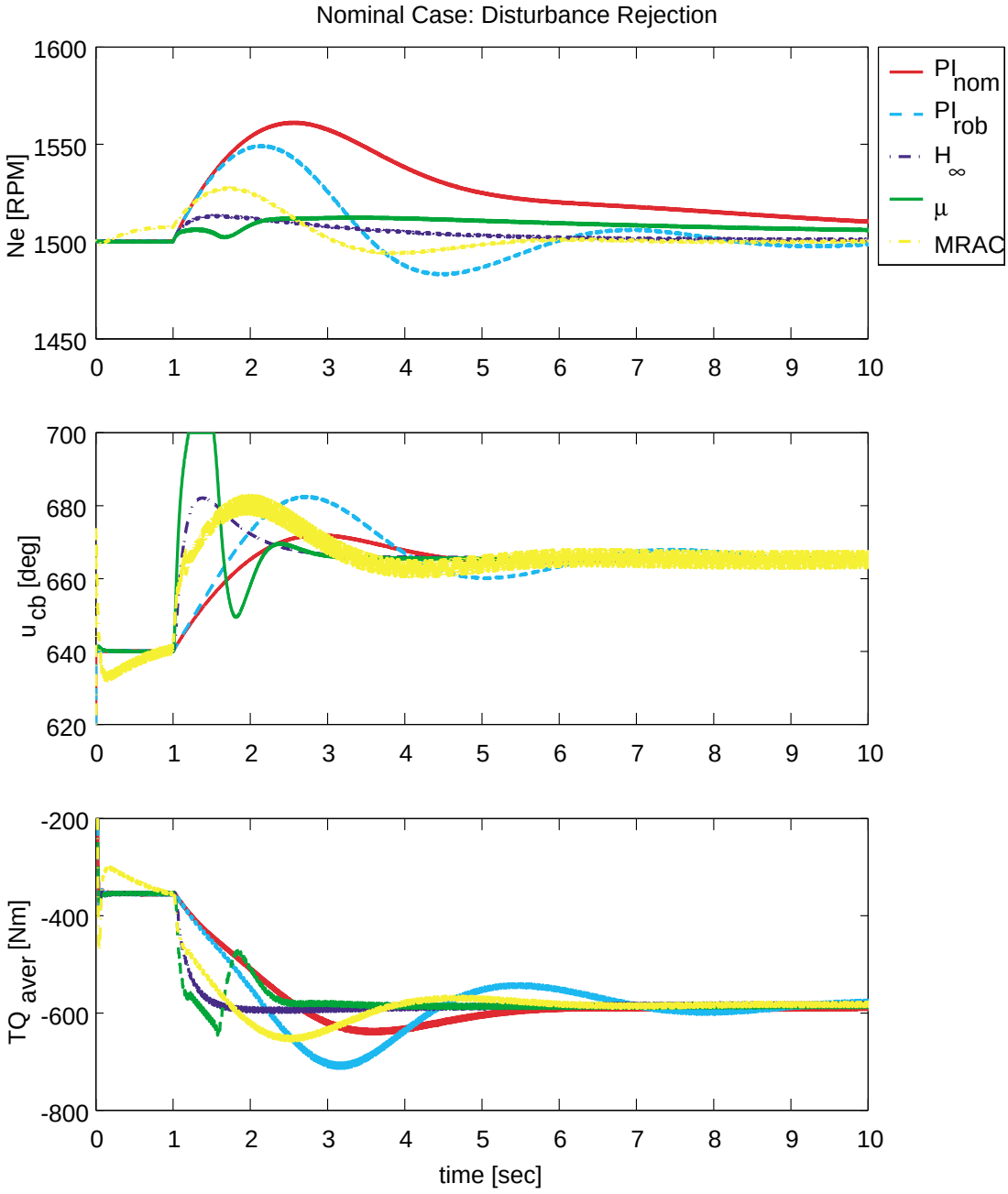


Figure 4.19: ***Nominal Vehicle Configuration:*** *Disturbance rejection capabilities for all the controllers.*

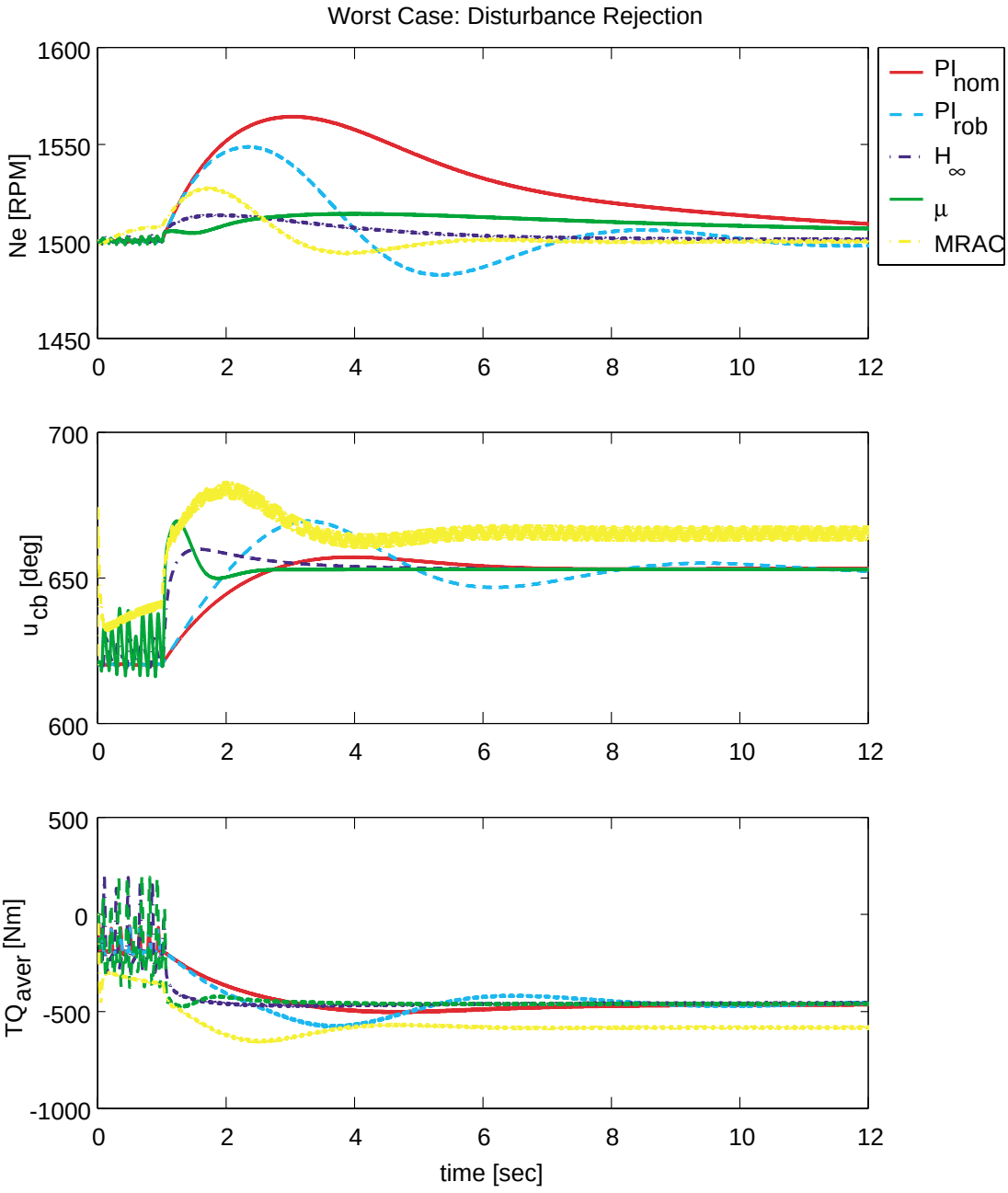


Figure 4.20: ***Worst Vehicle Configuration:*** *Disturbance rejection capabilities for all the controllers.*

## 4.6 Coordination with Gear Selection

For given vehicle mass, engine speed and road grade, there is a limitation to the amount of compression braking each selected gear number can provide. Neglecting the service brakes retarding power, (3.10) is formulated for steady state operations the following way:

$$TQ + r_g(F_\beta - F_a) = 0, \tag{4.26}$$

where $TQ$ is the compression braking torque, $r_g$ is the total gear ratio, $F_\beta$ given by (3.13) is the force due to the road grade, and $F_a$ is aerodynamic drag forces, given by (3.14). For simplicity, we present the equations again here:

$$\begin{aligned} TQ &= \alpha_0 + \alpha_1\tilde{\omega} + \alpha_2 W_b + \alpha_3 W_b\tilde{\omega} + \alpha_4\tilde{\omega}^2 + \alpha_5 W_b\tilde{\omega}^2 \\ F_\beta &= -r_g Mg(\cos\beta - f_r \sin\beta) \\ F_a &= \frac{1}{2}\rho c_d A_v r_g^2 \omega^2. \end{aligned}$$

To guarantee that the compression brake is sufficiently powerful for given vehicle configuration, we solve (4.26) in terms of the maximum feasible road grade $\beta_{max}$ that the compression brake system can handle for chosen gear selection:

$$\beta_{max} = \arctan\left(\frac{f_r(-2r_g f_r F_a - 2f_r TQ_{max} + 2\Xi)}{2(f_r^2+1)Mgr_g} + \frac{F_a r_g + TQ_{max}}{Mgr_g}\right) \tag{4.27}$$

where

$$\Xi = \sqrt{M^2 g^2 r_g^2 f_r^2 - 2F_a r_g TQ_{max} - TQ_{max}^2 - F_a^2 r_g^2 + M^2 g^2 r_g^2}$$

Road grade information can potentially be obtained by using a two-antenna GPS system for a least-square based estimation scheme [1], or by using a GPS system together with digital road maps. Assuming that the road grade is measured $\beta_m$, the gear switching can be done by the following rule: we downshift from gear number n to gear number $(n-1)$ if $\beta_m > \beta_{max}$. If gear number $(n-1)$ is insufficient for the compression brake system to handle the grade, we simply command yet another downshift to gear number $(n-2)$.

A graphical representation of (4.27) is shown in Figure 4.21. Specifically, we show as an example that for vehicle mass $M = 20,000$ kg, driving with an engine speed $N_e = 1500$ RPM, then for gear number 5, the maximum road grade the compression brake can compensate for is $\beta_{max} = -7^o$.

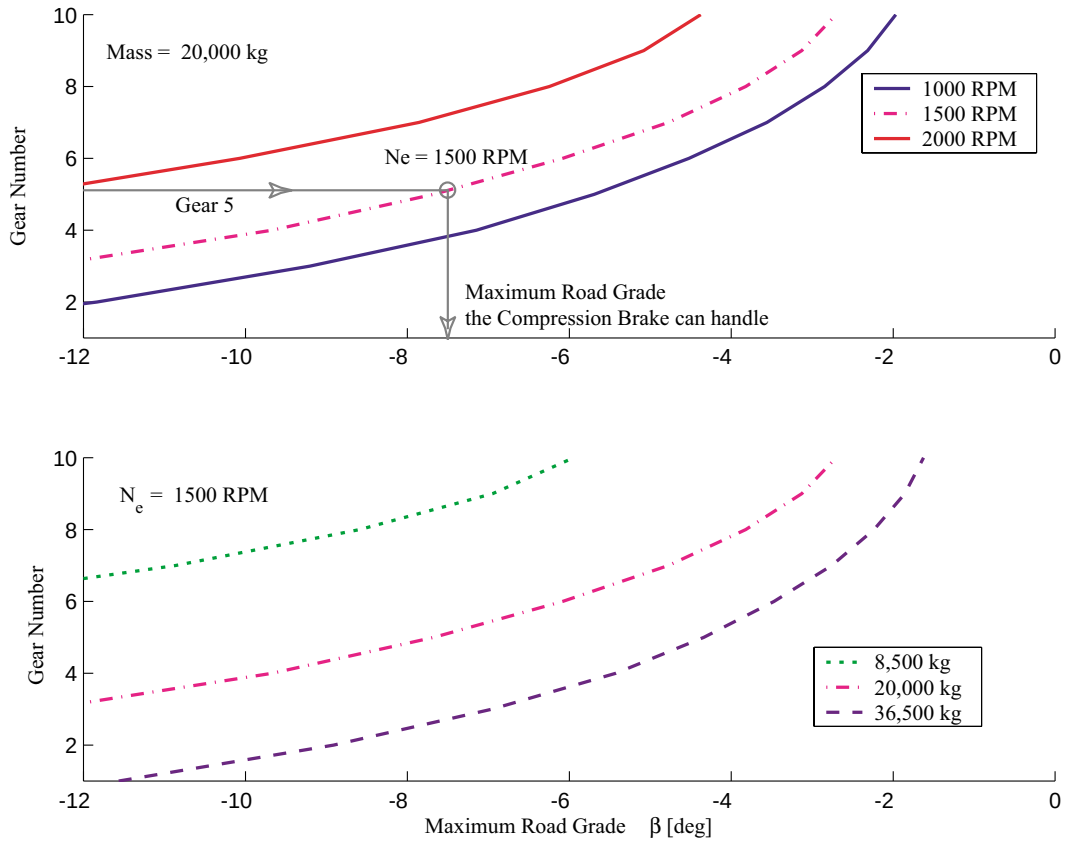


Figure 4.21: *For given vehicle mass and engine speed, there is a maximum road grade for what the compression brake can compensate, for each selected gear number.*

To demonstrate how coordination with gear selection works, we show in Figure 4.22 a CHV encountering a too steep road grade change from $\beta = -3.4^o$ to $-8.4^o$. The engine speed $\omega = 157$ rad/sec, the mass is 20,000 kg and gear selected is number 5. As shown in Figure 4.21, for this particular configuration, the maximum feasible grade the compression brake can handle without saturating is $\beta_{max} = -7^o$, hence, we down shift the gear from number 5 to number 4, as seen in Subplot 2. In this particular simulation, vehicle speed regulation is not the same as engine speed regulation due to a change in gear ratios. For desired vehicle speed shown in Subplot 5, we note an overshoot of approximately 10 %. The engine speed is shown in Subplot 4, and due to the change in gear ratio, the desired vehicle speed corresponds to two different levels of engine speed (dotted lines).

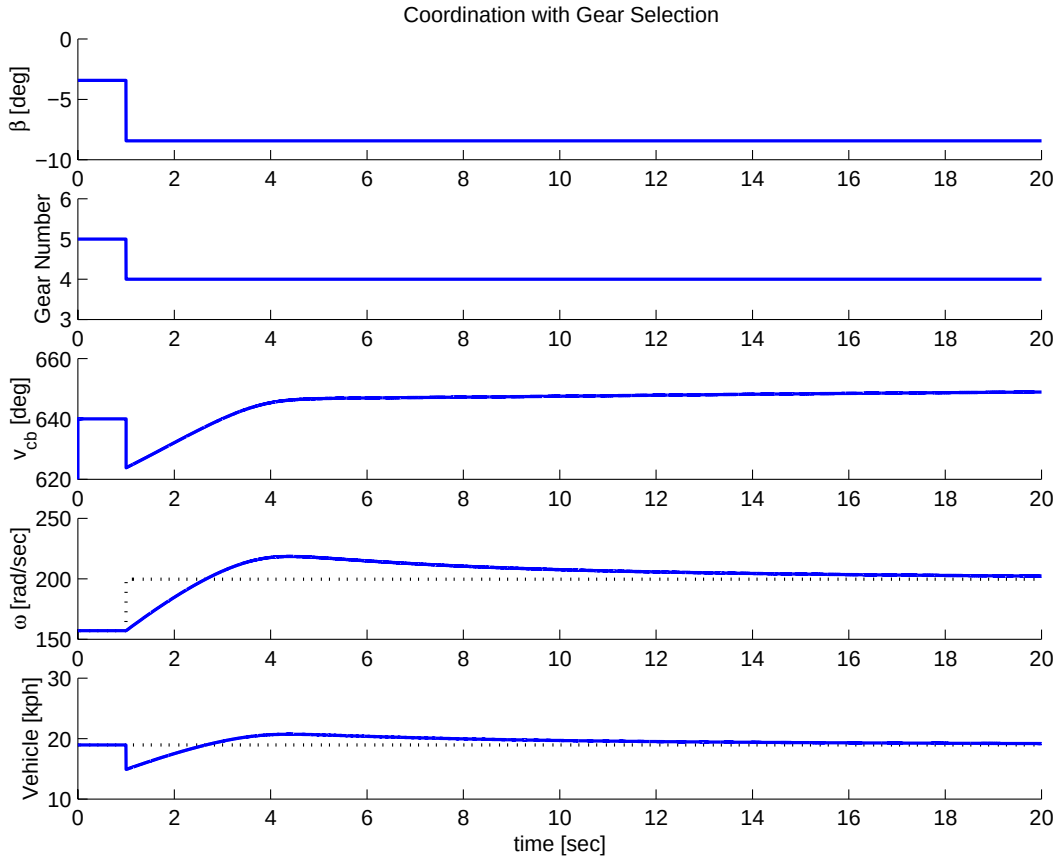


Figure 4.22: *Simulation show that the encountered grade is too large for the compression brake to handle for current gear selection, hence, a lower gear number is automatically selected to avoid saturation.*

In all the simulation scenarios we have presented so far, the use of the compression brake alone or coordinated with the proper gear selection has been sufficient to meet the speed tracking and control objectives. However, as shown in (4.27) there is a maximum limit on the compression braking capability. To alleviate this problem, we propose in Chapter 5, a coordinated braking controller design in which the service brakes are activated when the compression brake saturate.

## 4.7 Conclusion on Control Design

In this chapter, we design controllers employing classical and modern control techniques, for the vehicles system developed in the previous chapters. Initial linear simulations using standard PI–controllers, along with the analysis carried out in Chapter 3.3 indicate that better performance is achieved using robust or nonlinear controllers. Using the concept of structured singular values $\mu$, we design a 12th order $H_\infty$–controller and a 20th order $\mu$–controller using DK–iterations. In addition, we summarize work we have done on a model reference adaptive controller design. Through extensive simulations, using the 24th order nonlinear vehicle model, we demonstrate the performance of the controllers.

Although, the nominal PI–controller fails to meet the robust performance requirement ($\mu < 1$), its low order makes it a very good choice when it comes to practical implementation. The robust PI–controller, on the other hand, is most likely too oscillatory for any practical use. The $H_\infty$–controller is our second choice. It is of order 12, but this one, too, fails to meet the robust performance requirement. As for the $\mu$–controller, it satisfies the robust performance requirement, however, the high order of this one makes it unattractive. As for the model reference adaptive controller, more work has to be done to assess how sensitive the design is to the parameters in the open-loop torque observer. In addition, parameter estimation of mass and grade, although secondary to the speed control objective, is guaranteed on a reduced order model, as shown in Figure 4.15, under the persistence of excitation type of conditions. However, this is not achieved on the full nonlinear vehicle model, but is currently being investigated.

# Chapter 5

# Coordinated Braking Controller

In this chapter, we demonstrate the performance of coordinated braking controller (CBC) design through simulations of four driving scenarios. For the simulations we use the nominal PI–controller on the compression brake, but any of the other controllers discussed in the previous chapter will work as well.

To assess the improvements we achieve using the CBC design, we simulate four driving scenarios using the coordination of the compression brake and the service brakes. We then simulate the same scenarios with the compression brake disabled, using P–control on the service brakes only (SBO) as the sole retarding source.

## 5.1 Control Design

In Chapter 4, the following PI-controller for compression braking only is designed:

$$u_{cb}(t) = k_p \left( (\omega_c - \omega(t)) + \frac{1}{\tau_I} \int_0^t (\omega_c - \omega(\tau)) d\tau \right) + W_{b0}. \tag{5.1}$$

Coordination of the compression brake with the service brakes is achieved by using the following P–controller on the service brakes:

$$v_{sb}(t) = -k_{sb}(u_{cb} - sat_{min}(u_{cb})), \tag{5.2}$$

where $v_{sb}$, is the input to the service brake actuator as shown in Figure 5.1. Based on (5.2), the service brakes are activated when the control signal for compression brake (5.1) reaches its minimum value $sat_{min}(u_{cb}) = -100$. The

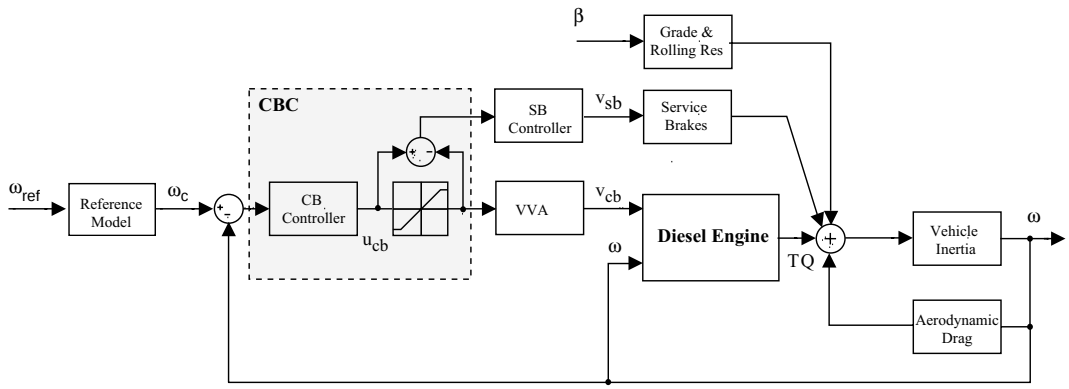


Figure 5.1: *Block diagram for coordinated braking controller (CBC) scheme.*

control strategy based on (5.1)–(5.2) assigns high priority to the compression brake and uses the service brakes only when absolutely necessary. This reduces the use of conventional service brakes, thus, reduces their wear and potentially maintenance costs.

For the tuning of the gain of the service brake controller, we still want to minimize steady state error between desired and measured speed and to minimize the effect of various disturbances. After several iterations of simulating the vehicle system when it saturates due to large step changes in road grade $\beta$, the following parameter is chosen: $k_{sb} = 0.1$.

To clearly illustrate how the coordination of the two braking mechanisms look like in terms of their controller signals, we show in Figure 5.2 the saturation of the control signal for compression brake $u_{cb}$ followed by the activation of the control signal for the service brakes $u_{sb}$, due to a large step change in road grade $\beta$. As seen in the lower plot, both the compression brake and the service brakes are activated to maintain the engine speed. After an initial speed excursion, the engine speed is regulated to desired level after 16 seconds.

In the next section, we demonstrate how the coordinated braking control design reduces the use of service brakes through simulations of four critical driving scenarios.

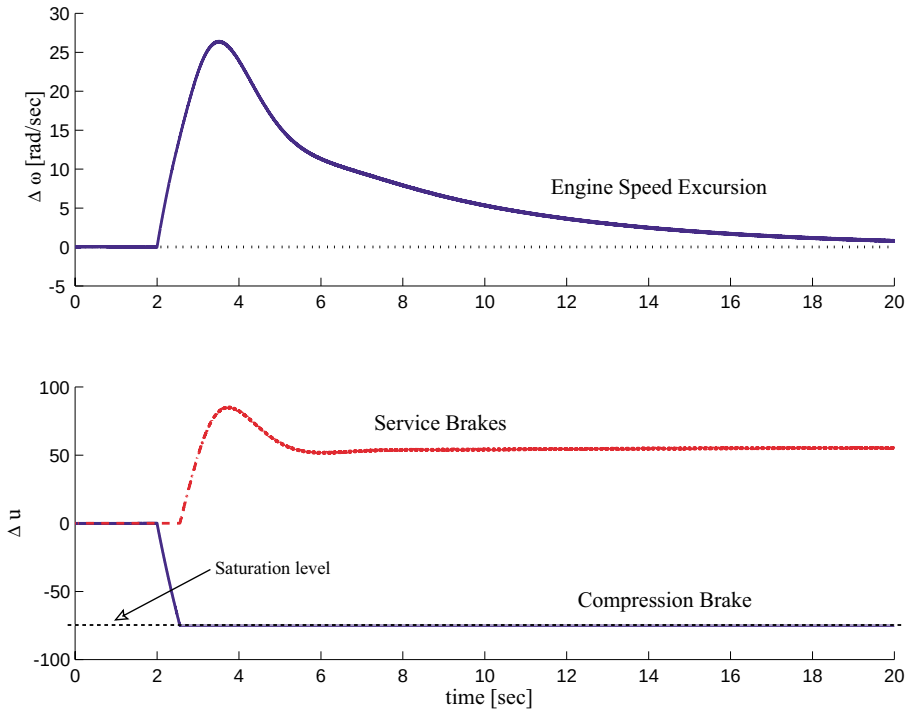


Figure 5.2: *Switching from combustion to braking mode.*

## 5.2 Simulations on Full Order Model

In this section, we demonstrate the performance of coordinated braking controller (CBC) design through simulations of four driving scenarios (DS). We use the nominal PI–controller on the compression brake, and the P–controller on the service brakes when they are engaged due to the saturation of the compression brake.

### 5.2.1 Driving Scenario 1:

The driving scenario shown in Figure 5.3, illustrates a CHV in braking mode, descending on a constant grade, $\beta = -2$ degrees (Subplot 1). The total gear ratio $r_g$ (here, corresponding to the fifth gear), is kept constant throughout the simulations. After two seconds, we command a step change in desired engine speed $\omega$ from 157 to 149 rad/sec (Subplot 5). The settling time is approximately 6 seconds. In the first driving scenario, we show simulation results using the full order nonlinear vehicle model in addition to a reduced order vehicle model

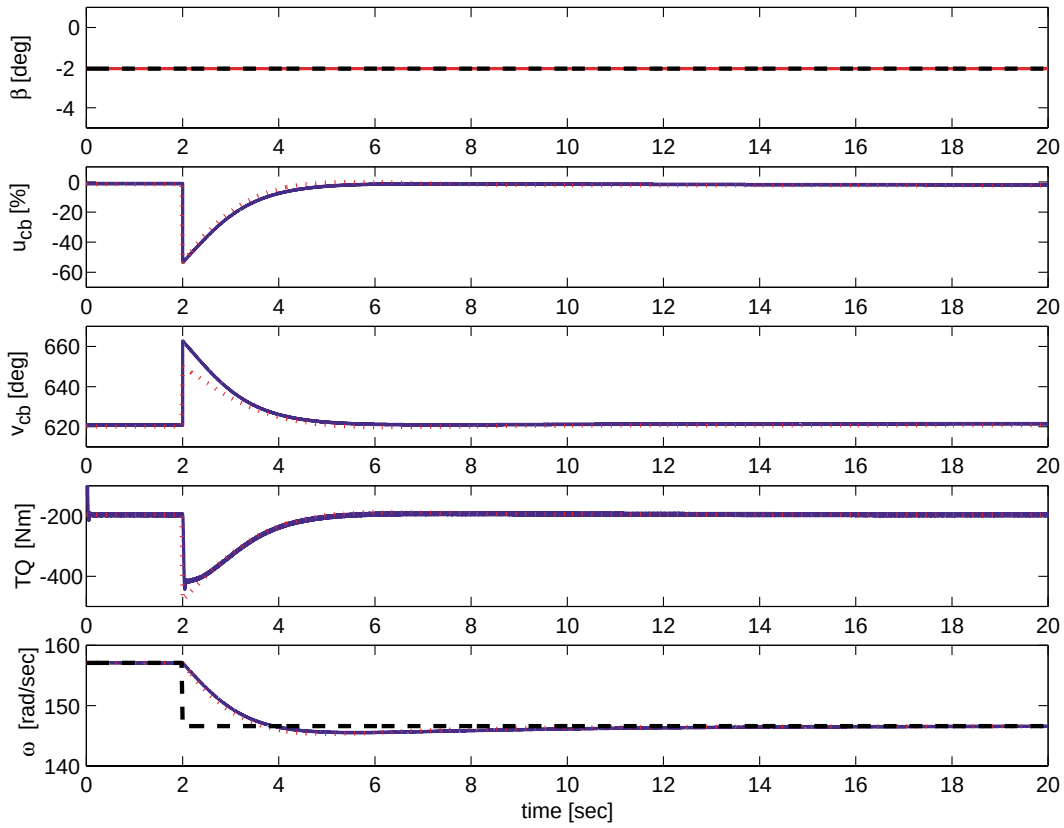


Figure 5.3: ***Driving Scenario 1:*** *Step change in desired engine speed from 157 to 149 rad/sec when operating in braking mode. Results from using the full order nonlinear vehicle model is show as solid lines, while results from using a reduced order model is shown as dotted lines.*

using the extracted linear engine dynamics. This is added to demonstrate that the model order reduction performed in [22] is good. Indeed the reduced order vehicle model is capable of capturing the dynamics the behavior of the nonlinear full order model for this particular driving scenario. Computation time for the full order vehicle model is approximately 20 minutes for 20 seconds of simulation, while the computing time for the reduced order model is only approximately 10 seconds.

### 5.2.2 Driving Scenario 2:

Figure 5.4 illustrates a CHV in braking mode, initially descending on a grade, $\beta = -3.4^o$ degrees (Subplot 1). After two seconds, the CHV encounters a step

change in grade from $-3.4^o$ to $-10.4^o$, which is too much for the compression brake to handle alone. Upon the saturation of the control signal for the compression brake $u_{cb}$ (Subplot 2), the service brakes are activated, as seen in the same Subplot. After an initial excursion, the engine speed in regulated to desired level after approximately 10 seconds.

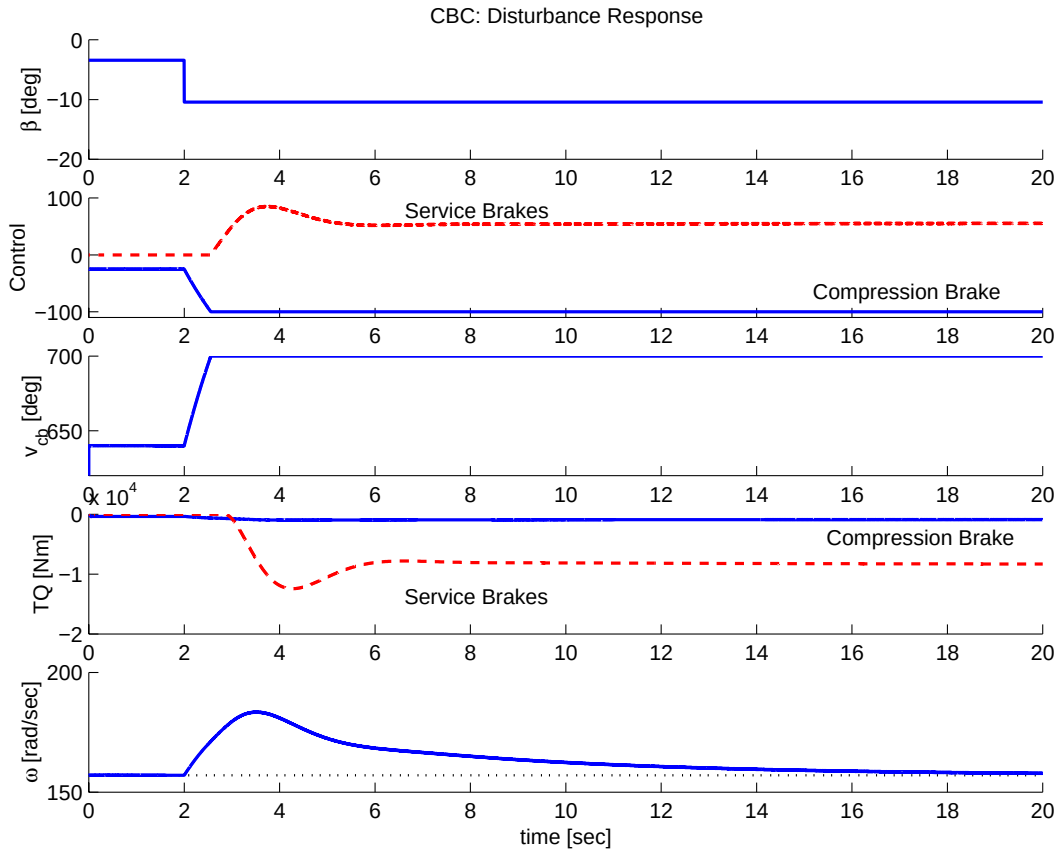


Figure 5.4: ***Driving Scenario 2:*** *Large step in grade while operating braking mode results in saturation of $u_{cb}$ which activates the service brakes.*

### 5.2.3 Driving Scenario 3:

Driving scenario 3, shown in Figure 5.5, shows the CHV performing a transition from combustion mode to braking mode. The truck is initially driving uphill for two seconds until it encounters a grade change from $\beta = 2.4^o$ to $\beta = -2.6^o$ as seen in Subplot 1. The compression brake is engaged (Subplot 3), and the engine

speed is regulated to desired level after approximately 10 seconds, without the use of service brakes.

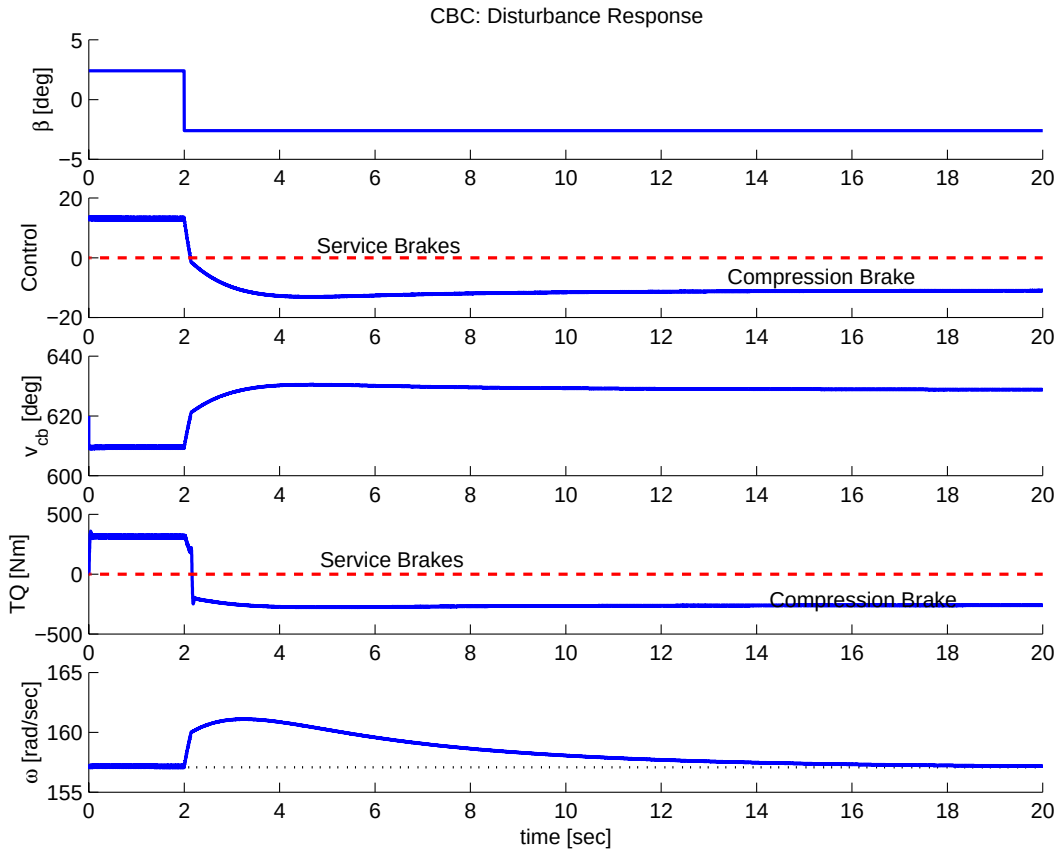


Figure 5.5: ***Driving Scenario 3:*** *Transition from combustion to braking mode due to a small step change in grade. Service Brakes are not engaged.*

### 5.2.4 Driving Scenario 4:

In the fourth and most demanding driving scenario, shown in Figure 5.5, the CHV is once again performing a transition from combustion mode to braking mode. The truck is initially driving uphill for two seconds until it encounters a very large grade change from $\beta = 2.4^o$ to $\beta = -7.6^o$ as seen in Subplot 1. However, the grade disturbance is too large for the compression brake, it saturates and thus engages the service brakes, as seen in Subplot 2. After approximately 10 seconds, the engine speed is regulated to desired level.

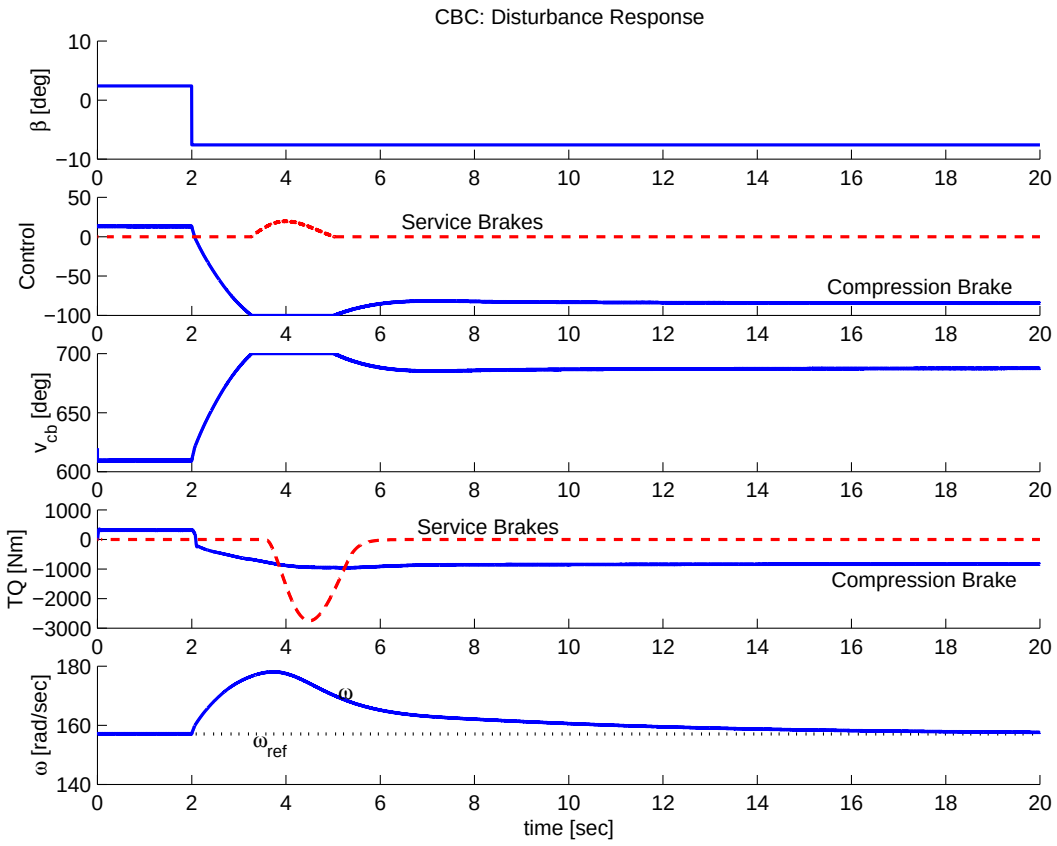


Figure 5.6: ***Driving Scenario 4:*** *Transition from combustion to braking mode due to a large step change in grade. The control output for the compression brake saturates and due to that, the service brakes are activated.*

In Figure 5.7 we show the corresponding phase plots of the retarding power versus vehicle speed for driving scenario 1 and 4, to demonstrate the importance of taking the dynamics into account when we perform engine speed equilibrium analysis.

## 5.3 Improvements using Coordination of Brakes

To quantify the improvements we achieve using the CBC controller scheme, we define the following performance index:

$$I = \int_0^{t_{set}} v_{sb}(\tau)^2 d\tau, \tag{5.3}$$

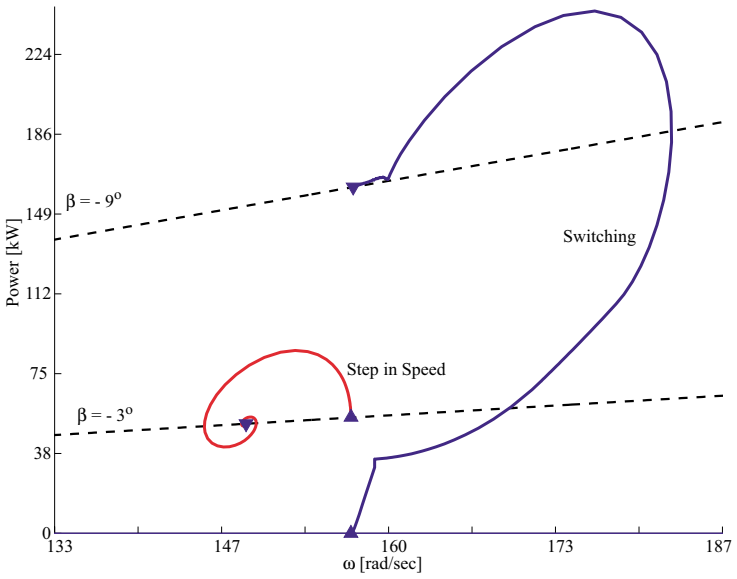


Figure 5.7: *Phase plots for driving scenario 1 and 4.*

where the settling time $t_{set}$ is defined as the time required for the service brake actuator signal $v_{sb}$ to reach and remain inside a band whose width is equal to $\pm$ 5 % of the new steady state value [24].

In driving scenario 2 and 4, the service brakes have to be used to regulate engine speed. Initial results using (5.3) indicates that the ratio between the use of service brakes for SBO and CBC is approximately 17.5 for DS 2, and 45 for DS 4. This means that using a coordinated braking controller scheme in critical longitudinal maneuvers, potentially reduces the use of service brakes by a factor of 45.

If we in addition to comparing performance indices, compare settling times $t_{set}$ for the same two driving scenarios, we find that $t_{set}$ is reduced from about 6.5 to about 4.2 seconds for DS 2, and from about 10 to 4 seconds for DS 4. Driving scenario 4, in which the CHV is going through a transition from combustion to braking due to a large step change in grade is a critical longitudinal maneuver, hence, a decrease in the settling time by a factor of 2 is substantial when it comes to reduction of wear and tear on the friction pads in the service brakes.

# Chapter 6

# Conclusions and Future Work

In Automated Highway Systems two major goals are to increase highway capacity and to enhance driving safety. The work presented in this report demonstrates that retarding power and retarding control are critical in accommodating higher operational speed and acceleration performance of modern Commercial Heavy Vehicles. The use of the compression brake in coordination with the service brakes increases the overall retarding power of the vehicle and reduces the maintenance cost of the service brakes. The compression brake can be used continuously without the danger of overheating, and is, thus, a natural actuator to be used for longitudinal speed control.

- Initial linear PI–controllers are designed to emulate the driver's actions to maintain desired vehicle speed during descends on long road grades.
- To account for the parameter variations and model uncertainty in the CHV, we employ robust control analysis techniques and design an $H_\infty$–controller and a $\mu$–controller.
- To effectively control the vehicle system for the large and unknown variations in mass and grade, a model reference adaptive controller is presented. Mass and grade estimations are proven to converge on a reduced vehicle model.

A natural extension of the work presented herein is to enhance safety during critical lateral maneuvers. One of the most common causes of highway accidents involving CHVs is the uncontrolled large relative yaw motion between the tractor and the trailer. Lateral control schemes which independently controls the

braking force on the outer and inner rear trailer wheels do already exists. However, due to the increase in operational speed, the conventional service brakes operated close to pressure limits. By coordinating the developed continuously variable compression brake with the conventional service brakes and the steering mechanism, we can potentially eliminate this safety problem.

# Bibliography


[1] Bae, H.S, amd Gerdes, J. "Parameter estimation and command modification for longitudinal control of heavy vehicles," *Proc. of International Symposium on Advanced Vehicle Control*, Ann Arbor, MI, Aug. 2000.

[2] BD. Exhaust Brake. Retrieved on: http://www.bd-vfi.com/Exhaust_Brakes/Turbo_Mount_Exhaust_Brake/, September 1999.

[3] Carlstrom. P. 1999. Volvo High Power Engine Brake. Retrieved on: http:/www.truck.volvo.se.

[4] Chen. C. and Tomizuka. M. "Steering and independent braking control for tractor-semitrailer vehicles in automated highway systems," *Proceedings of the 34th CDC*, 1995.

[5] Cummins. D. D. The Jacobs Engine Brake Application and Performance. *SAE*, (660740). 1966

[6] Diesel maker to do away with the camshaft. *Design News*, 7–3–00. 2000.

[7] Druzhinina M., Moklegaard L., Stefanopoulou A. Compression braking control for heavy duty vehicles. *Proc. of American Control Conference*. 2000.

[8] Druzhinina M., Moklegaard L., Stefanopoulou A. Speed gradient approach to longitudinal control of heavy duty vehicles equipped with compression brake. *Proc. of International Symposium on Advanced Vehicle Control*. Ann Arbor, Michigan. 2000.

[9] Druzhinina M., Moklegaard L., Stefanopoulou A. Speed gradient approach to longitudinal control of heavy duty vehicles equipped with variable compression brake. *Submitted to IEEE Transactions on Control System Technology*. 2000.

[10] Druzhinina M., Stefanopoulou A., and Moklegaard L. Adaptive Continuously Variable Compression Braking Control for Heavy–Duty Vehicles. *Submitted to Journal of Dynamic Systems, Measurement, and Control*. 2000.

[11] Fitch. J. W. *Motor Truck Engineering Handbook*. SAE Inc., 4th. edition. 1994.

[12] Gerdes C. J., Brown S. A., and Hedrick. K. J. "Brake System Modeling for Vehicle Control," *Advanced Automotive Technologies - 1995 ASME IMECE,* pp.105-112. 1995.

[13] Hu. H., Israel. M. A., and Vorih. J. M. Variable Valve Actuation and Diesel Engine Retarding Performance. *SAE*, (970342). 1997.

[14] Hu. H., Vorih. J., and Israel. M. Lost-Motion VVT Diesel Engine Retarder. *Automotive Engineering International*, Jan, 1998.

[15] Jacobs Vehicle System. Intebrake Engine Braking Systme for Signature 600. Retrieved on: http:/www.jakebrake.com/products/engine. 1999.

[16] Jacobs Vehicle Systems. "Driveline Brakes". Retrieved on: http://www.jakebrake.com/. 1999.

[17] John Deere. Sharing the Road Media Group. Retrieved on: http://www.deere.com/truckerimage/sharing.

[18] Kanellapooulos. I. Integrated Longitudinal Control for Safe Automation of Commercial Heavy Vehicles. Proposal for the awarded MOU 393. 1999.

[19] Krstic, M., Kanellakopoulos, I., and Kokotovic, P. V. *Nonlinear and Adaptive Control Design*, Wiley, 1995.

[20] Moklegaard L., Druzhinina M., Stefanopoulou A. Brake valve timing and fuel injection: a unified engine torque actuator for Heavy-Duty Vehicles. *5th International Symposium on Advanced Vehicle Control*, Ann Arbor. 2000.

[21] Moklegaard. L., Schmidt. J., and Stefanopoulou. A. G. Transition from Combustion to Variable Compression Braking. *SAE*, (2000-01-1228). 2000.

[22] Moklegaard, L., Druzhinina , M., and Stefanopoulou, A., 2001, "Compression braking for longitudinal control of Commercial Heavy Vehicles," PATH Research Report UCB-ITS-PRR-2001-11.

[23] Raza. H., Xu. Z., and Yang. B. Brake Modeling for AVCS Application. Technical Report 94-01-01. PATH. 1994.

[24] Seborg. D. E., Edgar. T. F., and Mellichamp. D. A. *Process Dynamics and Control*. John Wiley & Sons, Inc. 1989.

[25] Shladover. S. E., Desoer. C. S., Hedrick. J. K., Tomizuka. M., Walrand. J., Zhang. W. B., McMahon. D., Peng. H., Sheikholeslam. S., and McKeown. N. Automatic Vehicle Control Developments in the PATH Program. *IEEE Trans. on Vehicular Technology*. 40(1):114–130. 1991.

[26] Skogestad. S. and Postlethwaite. I. *Multivariable Feedback Control Analysis and Design*. John Wiley & Sons. 1996.

[27] Yanakiev. D. and Kanellakopoulos. I. "Longitudinal control of automated CHVs with significant actuator delays," *Proceedings of the 36th CDC*, San Diego. pp. 4756-4763. 1997.

# Appendix A

# Nomenclature

In the following table, the symbol † indicates a variable where $x$ is replaced with: $f$ for front exhaust manifold, $r$ for rear exhaust manifold and $c$ for collector exhaust manifold.

| | |
|---|---|
| $\beta$ | road grade ($^o$) |
| $\eta_c$ | compressor efficiency |
| $\eta_t$ | turbine efficiency |
| $\gamma$ | specific heat ratio of air |
| $\mu$ | rolling resistance |
| $\omega$ | engine speed (rad/sec) |
| $\psi$ | standard orifice flow function |
| $\rho$ | air density (kg/$m^3$) |
| $\theta$ | crank angle ($^o$) |
| $A$ | frontal area of the truck ($m^2$) |
| $B$ | cylinder bore (m) |
| $BVT$ | Brake Valve Timing |
| $C_d$ | drag coefficient |
| $c_p$ | specific heat capacity for constant pressure (J/kg K) |
| $c_v$ | specific heat capacity for constant volume (J/kg K) |
| $C_q$ | quadratic resistive coefficient |
| $EM$ | exhaust manifold |
| $F_\beta$ | gravity force due to grade (N) |
| $F_{sb}$ | friction brake force (N) |
| $F_{qdr}$ | aerodynamic force (N) |
| $F_r$ | rolling resistance force (N) |

| | |
|---|---|
| $g_f$ | differential gear ratio |
| $g_t$ | transmission gear ratio |
| $IM$ | intake manifold |
| $I_{tc}$ | mass polar moment of inertia (Nm $sec^2$) |
| $J_e$ | engine inertia (Nm $sec^2$) |
| $J_t$ | total vehicle inertia (Nm $sec^2$) |
| $m_{cyl_j}$ | mass, cylinder j (kg) |
| $m_{e_x}$ † | mass, EM (kg) |
| $N_e$ | engine speed (RPM) |
| $N_tc$ | turbocharger speed (RPM) |
| $p_{cyl_j}$ | pressure, cylinder j (Pa) |
| $p_{e_x}$ † | pressure, EM (Pa) |
| $p_0$ | ambient pressure (Pa) |
| $P_c$ | compressor power (W) |
| $P_t$ | turbine power (W) |
| $Q_{ht}$ | heat transfer (J/sec) |
| $Q_{lhv}$ | lower heating value for diesel fuel (J/kg) |
| $r$ | crank radius (m) |
| $R$ | gas constant (J/kg K) |
| $r_\omega$ | wheel radius (m) |
| $r_c$ | compression ratio |
| $r_g$ | total rear ratio |
| $T_{cyl_j}$ | temperature, cylinder j (K) |
| $T_{e_x}$ † | temperature, EM (K) |
| $t_{sb}$ | service brake time constant (sec) |
| $T_0$ | ambient temperature (K) |
| $T_c$ | compressor temperature (K) |
| $T_i$ | temperature, IM (K) |
| $TQ$ | averaged engine torque (Nm) |
| $TQ_{shaft}$ | engine shaft torque (Nm) |
| $TQ_{cyl_j}$ | torque contribution from cylinder j (Nm) |
| $u_{sb}$ | output from service brake controller |
| $v$ | vehicle speed (m/sec) |
| $V_{cyl_j}$ | volume, cylinder j ($m^3$) |
| $\dot{V}_{cyl_j}$ | rate of change in volume, cylinder j ($m^3/sec$) |

| | |
|---|---|
| $V_{e_x}$ † | volume EM ($m^3$) |
| $V_{e_x}$ † | volume, EM ($m^3$) |
| $v_{cb}$ | brake valve timing ($^o$) |
| $v_{sb}$ | service brake air pressure (Pa) |
| $v_f$ | fuel flow (kg/sec) |
| $V_i$ | volume IM ($m^3$) |
| $W^B$ | unified engine signal corresponding to brake valve timing |
| $W^F$ | unified engine signal corresponding to fuel flow |
| $W_{afb_j}$ | apparent fuel burn rate, cylinder j (kg/sec) |
| $W_{cyl_j e_x}$ † | mass air flow from cylinder j into EM (kg/sec) |
| $W_{cyl_j i}$ | mass air flow from cylinder j into IM (kg/sec) |
| $W_{e_c e_f}$ | mass air flow from collector to front EM (kg/sec) |
| $W_{e_c e_r}$ | mass air flow from collector to rear EM (kg/sec) |
| $W_{e_f e_c}$ | mass air flow from front to collector EM (kg/sec) |
| $W_{e_r e_c}$ | mass air flow from rear to collector EM (kg/sec) |
| $W_{e_x cyl_j}$ † | mass air flow EM into cylinder j (kg/sec) |
| $W_{fb_j}$ | fuel burned rate, cylinder j (kg/sec) |
| $W_{icyl_j}$ | mass air flow from IM into cylinder j (kg/sec) |
| $W_{icyl_j}$ | mass air flow from IM into cylinder j (kg/sec) |
| $W_c$ | compressor mass flow (kg/sec) |
| $W_t$ | turbine mass flow (kg/sec) |

# Appendix B

# Braking Mode: Parameterization of Dynamics

Based on standard regression techniques, we employ the following parameterizations for the reduced order engine model described in Chapter 3.

We approximate the static torque for compression braking using the following second order polynomial:

$$TQ(t) \;=\; [1 \quad \tilde{\omega}(t) \quad W_b(t) \quad W_b(t)\tilde{\omega}(t) \quad \tilde{\omega}(t)^2 W_b(t) \quad \tilde{\omega}(t)^2] \quad \cdot\alpha$$

where

$$\alpha^T = [-7.932 \cdot 10^3, 9.894, 13.070, -1.600 \cdot 10^{-2}, -5.221 \cdot 10^{-3}, 8.460 \cdot 10^{-6}].$$

The regression is shown in Figure B.1, where the overall standard deviation of is 42.2 Nm, the mean is 11.5, and the maximum absolute error is less than 15 percent.

For the transfer function constants described in (3.3) and (3.6), we approximate the dynamics with the following set of polynomials:

$$\begin{aligned} \tau_\omega &= \mathcal{P}_{B1}(\omega_0, W_{b0}) = [1, \omega_0, W_{b0}, \omega_0 \cdot W_{b0}, \omega_0^2]\, b_4 \\ b_4 &= \begin{pmatrix} 2.497 \cdot 10^1 \\ -9.108 \cdot 10^{-3} \cdot \frac{30}{\pi} \\ -3.734 \cdot 10^{-2} \\ 1.602 \cdot 10^{-5} \cdot \frac{30}{\pi} \\ -6.871 \cdot 10^{-7} \cdot (\frac{30}{\pi})^2 \end{pmatrix} \end{aligned}$$

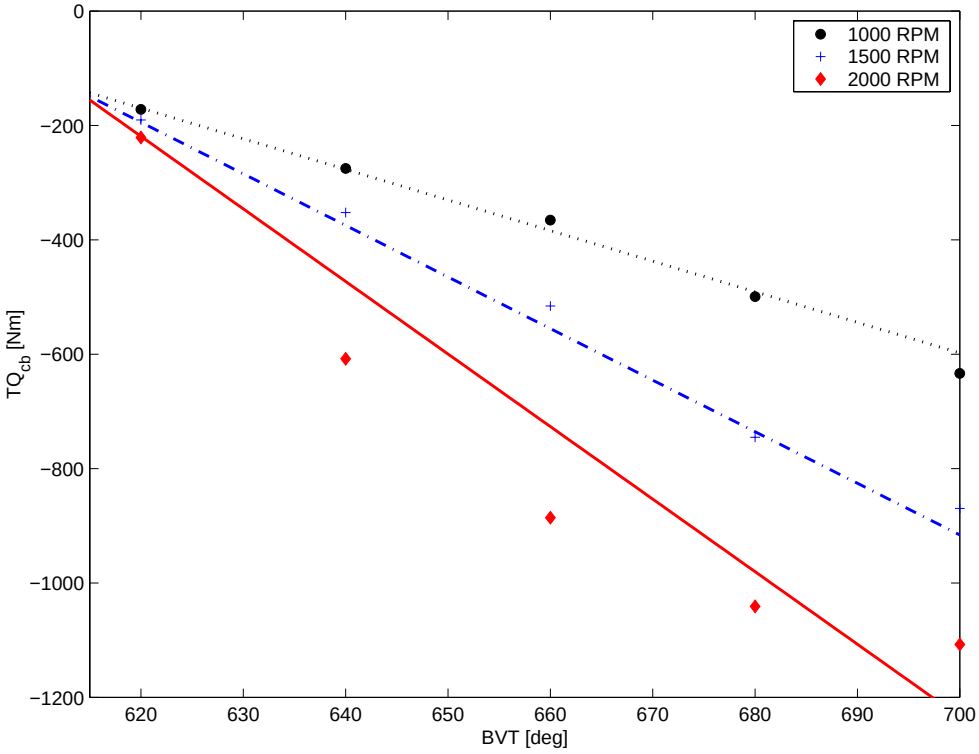


Figure B.1: *Regression of compression braking torque.*

$$
\begin{aligned}
c_\omega &= \mathcal{P}_{B2}(\omega_0, W_{b0}) = [1, \omega_0, W_{b0}, \omega_0 \cdot W_{b0}, \omega_0^2]\, b_5 \\
b_5 &= \begin{pmatrix} 1.267 \cdot 10^{1} \\ -6.586 \cdot 10^{-3} \cdot \frac{30}{\pi} \\ -1.711 \cdot 10^{-2} \\ 8.225 \cdot 10^{-6} \cdot \frac{30}{\pi} \\ 2.486 \cdot 10^{-7} \cdot (\frac{30}{\pi})^2 \end{pmatrix}
\end{aligned}
$$

$$
\begin{aligned}
\tau &= \mathcal{P}_{B3}(\omega_0, W_{b0}) = [1, W_{b0}, \omega_0, \omega_0 \cdot W_{b0}, W_{b0}^2]\, b_2 \\
b_2 &= \begin{pmatrix} 1.435 \cdot 10^{2} \\ -3.784 \cdot 10^{-1} \\ -1.468 \cdot 10^{-2} \cdot \frac{30}{\pi} \\ 2.044 \cdot 10^{-5} \cdot \frac{30}{\pi} \\ 2.501 \cdot 10^{-4} \end{pmatrix}
\end{aligned}
$$

$$
\begin{aligned}
c &= \mathcal{P}_{B4}(\omega_0, W_{b0}) = [1, W_{b0}, \omega_0, \omega_0 \cdot W_{b0}, W_{b0}^2]\, b_3 \\
b_3 &= \begin{pmatrix} 7.075 \cdot 10^{1} \\ -1.649 \cdot 10^{-1} \\ -1.311 \cdot 10^{-2} \cdot \frac{30}{\pi} \\ 1.861 \cdot 10^{-5} \cdot \frac{30}{\pi} \\ 9.176 \cdot 10^{-5} \end{pmatrix}
\end{aligned}
$$

$$
\tau_a = \mathcal{P}_{B5}(\omega_0, W_{b0}) = 10 \cdot 10^{-3}
$$

Figure B.2 shows the regression for the transfer function constants, while Table B.1 outlines the statistics for the regression.

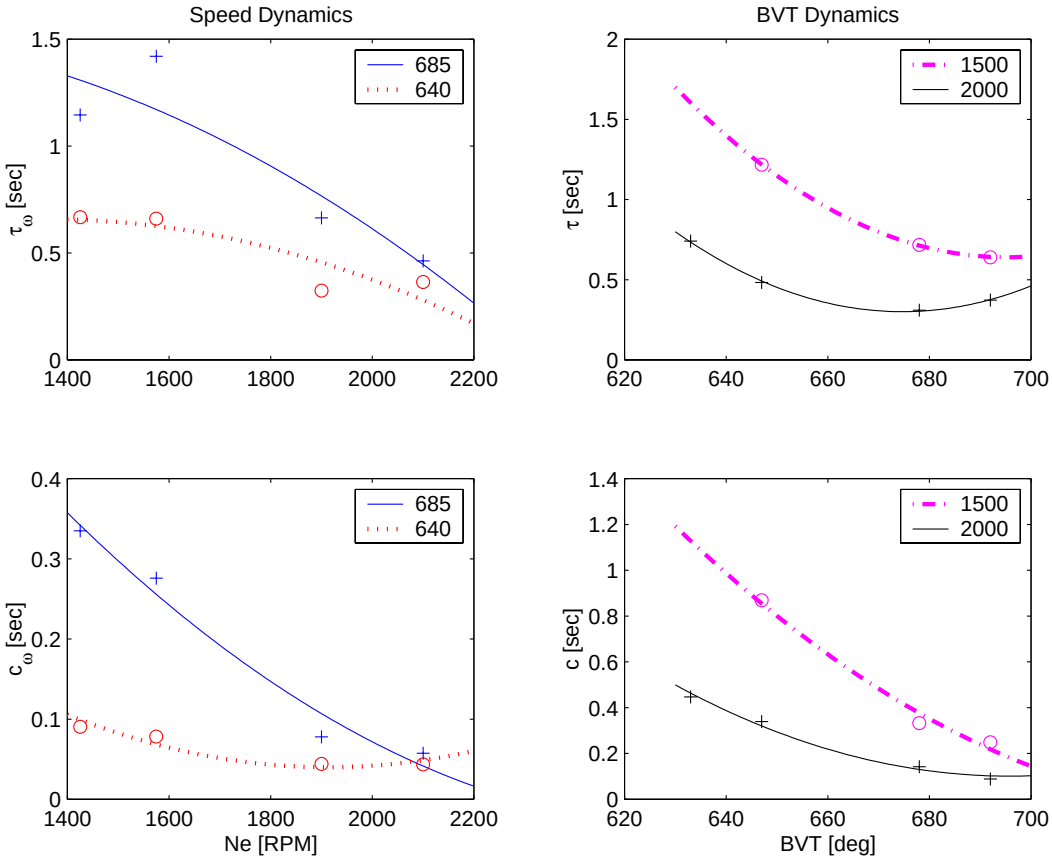


Figure B.2: *Regression of the poles and zeros for the compression brake mode.*

| | standard deviation | mean | maximum absolute error |
|---|---|---|---|
| $\tau$ | 0.006 | 0 | -2 % |
| c | 0.03 | 0 | -13 % |
| $\tau_\omega$ | 0.13 | 0 | 17.5 % |
| $c_\omega$ | 0.02 | 0 | -37 % |

Table B.1: **Braking Mode:** Statistics for regression of poles and zeros.